Copy 7
RM E50D05







NACA

# RESEARCH MEMORANDUM

## EXPERIMENTAL INVESTIGATION OF SUPERSONIC FLOW WITH DETACHED SHOCK WAVES FOR MACH NUMBERS BETWEEN 1.8 AND 2.9

By W. E. Moeckel

Lewis Flight Propulsion Laboratory
Cleveland, Ohio



NATIONAL ADVISORY COMMITTEE
FOR AERONAUTICS

WASHINGTON
July 5, 1950

NATIONAL ADVISORY COMMITTEE FOR AERONAUTICS

RESEARCH MEMORANDUM

# EXPERIMENTAL INVESTIGATION OF SUPERSONIC FLOW WITH DETACHED SHOCK WAVES FOR MACH NUMBERS BETWEEN 1.8 AND 2.9

By W. E. Moeckel

## SUMMARY

Results of an experimental investigation of the flow near the nose of plane and axially symmetric bodies in the presence of detached shock waves are compared with predictions of theory. The location of the detached shock wave was determined from schlieren photographs for a variety of nose shapes over a range of free-stream Mach numbers from 1.8 to 2.9. At a Mach number of 1.9, the form of the detached wave and the pressure distribution over the body were investigated for each nose shape. In addition, the relation between shock location and flow spillage was determined for several axially symmetric nose inlets.

In the range of Mach numbers investigated, the shock location was found to be predictable to good approximation by existing theory. At a Mach number of 1.9, the drag of the bodies upstream of their estimated sonic points also agreed reasonably well with predicted results. For most of the bodies investigated, the form of the detached shock wave at a Mach number of 1.9 was represented to good approximation by an hyperbola asympotic to the free-stream Mach waves. The flow spillage for the nose inlets, as predicted from shock location, agreed closely with values obtained by other means.

## INTRODUCTION

A simple approximate method for predicting the location of detached shock waves ahead of arbitrary plane and axially symmetric bodies in supersonic flow is derived in reference 1. The method consists in applying the one-dimensional continuity relation to a simplified representation of the flow field. An estimate of the pressure drag of the portion of the body upstream of its estimated sonic points is also presented, together with an expression for the relation between shock location and flow spillage for nose inlets.

Experimental data in the field of supersonic flow with detached shock waves have, until recently, been very meager. Results presented in reference 2 are substantial contributions to this field but are confined to cones and spheres and contain no information on drag. The data on shock location in reference 2 agree well with the predictions of reference 1.

An investigation was undertaken at the NACA Lewis laboratory to provide further checks on the accuracy of the method presented in reference 1. (A résumé of this method is presented in appendix A.) The location of the shock wave relative to the body was obtained for a wide variety of plane and axially symmetric nose forms over a range of Mach numbers from 1.8 to 2.9. A more detailed investigation, which included determination of the form of the detached waves and the drag for each body, was conducted at a Mach number of 1.9.

## SYMBOLS

The following symbols, some of which are illustrated in figure 1, are used herein:

A area

B $\sigma\left(\frac{P_0}{P_s}\right)_c$

b span

C $\beta\left(\beta \tan \varphi_s - \sqrt{\beta^2 \tan^2 \varphi_s - 1}\right)$

$C_D$ drag coefficient (based on area indicated by subscript)

$C_p$ pressure coefficient, $\frac{p-p_0}{\frac{1}{2}\rho_0 V_0^2}$

$k = \frac{1}{\gamma M_0^2}\left[1.2679\left(\frac{P_s}{P_0}\right)_c \frac{P_0}{p_0} - 1\right]$

| | |
|---|---|
| $L$ | distance in free-stream direction between vertex of detached wave and sonic point on body |
| $M$ | Mach number |
| $P$ | stagnation pressure |
| $p$ | static pressure |
| $R$ | maximum radius of axially symmetric bodies |
| $T$ | thickness |
| $t$ | $T/2$ |
| $V$ | velocity |
| $x$ | coordinate in free-stream direction |
| $y$ | coordinate perpendicular to free-stream direction |
| $\alpha$ | angle of attack |
| $\beta$ | $\sqrt{M_0^2-1}$ |
| $\gamma$ | ratio of specific heats (1.4 for air) |
| $\eta$ | inclination of sonic line with respect to y-axis |
| $\theta_d$ | cone half-angle for which shock becomes detached |
| $\lambda_d$ | two-dimensional shock detachment angle |
| $\lambda_s$ | streamline angle at sonic point of detached shock |
| $\rho$ | density |
| $\sigma$ | isentropic ratio of critical area to free-stream area |
| $\tau$ | fraction of maximum possible inlet mass flow that passes outside cowl |
| $\varphi$ | local inclination of detached shock wave relative to x-axis |

[redacted]

Subscripts:

| | |
|---|---|
| 0 | free-stream condition |
| c | centroid of stream tube passing sonic line |
| m | streamline that separates flow entering an open-nose body from external flow |
| S | sonic point on detached wave |
| SB | estimated sonic point on body |
| s | condition at sonic line |
| 1 | upper half of unsymmetrical configuration |
| 2 | lower half of unsymmetrical configuration |

## APPARATUS AND MODELS

The principal portion of the experimental program was conducted in the 18- by 18-inch supersonic tunnel at a test-section Mach number of 1.9. The models used are indicated schematically in figure 2, where the bodies designated A have rectangular cross sections and the bodies designated B are axially symmetric. The form of the bodies upstream and downstream of the estimated sonic point was varied in each group. The coordinates for bodies A-7 and B-6 are given in table I.

The A-bodies were 10 inches wide for most tests in the 18- by 18-inch tunnel, so that the ratio of span to thickness $b/T$ was 6.16 for bodies A-1 to A-4 and 4.0 for bodies A-5 to A-7. Although these bodies have finite span, they are referred to as "plane" or "two-dimensional" for convenience. Additional tests were made with body A-2 to check the effect of $b/T$ on shock form and location. For these tests, body A-2 was cut to widths of 7.5 and 5 inches, which correspond to values of $b/T$ of 4.62 and 3.07, respectively. Larger values of $b/T$ than 6.16 were not feasible in this investigation because an increase in span would have choked the tunnel at very low angles of attack, whereas a decrease in thickness would have reduced the accuracy of measurements from schlieren photographs. In order to attain a closer approximation to two-dimensional flow, body A-2 was therefore fitted with end plates for one test. These

[redacted]

end plates projected upstream of the leading edge of the body to the expected location of the detached wave and the upstream edges of the plates were cut to follow closely the expected contour of the shock wave. The passage of mass flow around the ends was thus reduced to a minimum, consistent with the requirement that the detached wave must be visible in the schlieren photographs.

All models investigated in the 18- by 18-inch tunnel were instrumented with static-pressure tubes to measure the surface pressure distributions. For the plane bodies, pressure orifices were located midway between the ends in the streamwise direction on both surfaces and around the leading edge. For the axially symmetric bodies, the pressure orifices lay in a plane through the axis of symmetry, and angle-of-attack effects were determined by rotating the bodies in this plane.

Another series of models was constructed for investigation in the variable Mach number tunnel described in reference 3. The test section of this tunnel is 4 by 4 inches at a Mach number of 2.0 and becomes larger or smaller as the Mach number is increased or decreased. For this investigation, the contours shown in figure 2 were used, but the maximum thicknesses and diameters were reduced to 0.5 inch. The A-group in this series was 1.5 inches in span, so that $b/T$ for these models was 3.0. No pressure instrumentation was attempted for these models. All models in both tunnels were sting-supported from the rear.

## RESULTS AND DISCUSSION

Schlieren photographs. - Typical schlieren photographs of the models tested in the 18- by 18-inch tunnel are shown in figure 3. Figures 3(a) to 3(f) are representative of the configurations obtained for the plane bodies at zero angle of attack and at the maximum angle of attack for which the portion of the detached wave between its sonic points was estimated to remain unaffected by the tunnel wall. For angles of attack slightly greater than those shown, choking occurred in the passage between the model and the wall.

The analogous configurations for the axially symmetric bodies are shown in figures 3(g) to 3(l). The A and B configurations are seen to produce similar flow patterns, except that the detached wave is considerably closer to the nose in the B-group. The thickness of the shock appears to be greater for the A-bodies than for the B-bodies. This effect is believed to result from a slight

misalinement of the A-bodies with respect to the light rays. In analyzing the data, the upstream boundary of the detached shock wave was used in measuring shock location and shock form.



Representative nose inlets with detached shock waves are shown in the schlieren photographs of figures 3(m) to 3(p). These photographs were taken in connection with other investigations (references 4 to 6) and depict typical off-design flow patterns.

Schlieren photographs taken in the variable Mach number tunnel are not shown because they were, in general, rather indistinct in the region close to the detached wave and near the nose of the bodies. This indistinctness introduced a considerable experimental error in the shock locations measured in these tests and prevented an accurate determination of shock form as a function of Mach number.

Shock-location parameter. - The experimental variation of shock-location parameter $L/y_{SB}$ with free-stream Mach number $M_0$ for each of the bodies investigated is shown in figure 4. The values obtained in the 18- by 18-inch tunnel are given in table II, and some of these values are also plotted in figure 4 for comparison with the variable Mach number tunnel results.

For the axially symmetric bodies (fig. 4(a)), the variation of shock-location parameter with Mach number follows the predicted variation reasonably well, but the curve obtained by the continuity method lies near the lower limit rather than near the mean of the values obtained. The geometric method, as expected, predicts values of $L/y_{SB}$ that are higher than those obtained with any of the bodies investigated, although at the highest Mach number, where the shock ahead of B-3 is approaching attachment, the value predicted by the geometric method is close to that experimentally obtained. The high value obtained for B-5 at a Mach number of 2.9 can probably be attributed to experimental error. This error, which was introduced by the fuzziness of the photographs obtained with the schlieren system of the variable Mach number tunnel, varied from one photograph to another but is estimated to average between 2 and 5 percent. Other evidence of experimental scatter is seen in comparing the values of $L/y_{SB}$ obtained for bodies B-2, B-4, B-5, and B-6. Inasmuch as the nose forms upstream of the sonic point are the same for these models, the shock-location parameters were also expected to be the same. This expectation was more nearly realized in the 18- by 18-inch tunnel tests (table II).

[redacted]

The difference shown in figure 4(a) between the results obtained in the variable Mach number tunnel and those obtained in the 18- by 18-inch tunnel at a Mach number of 1.9 may indicate a Reynolds number effect, but it seems unlikely that the difference in boundary-layer thickness is sufficient to account entirely for the observed differences in $L/y_{SB}$. Most of the difference must probably be attributed to experimental error in the variable Mach number tunnel results.

For the plane bodies (fig. 4(b) and table II), all experimental results with finite span-thickness ratio fall considerably below the predicted values. This result is to be expected because some of the air that would cross the two-dimensional sonic line passes around the edges of these models and consequently allows the shock wave to move closer to the nose. The effect of increasing $b/T$ for some of these bodies, and hence reducing the percentage of air that passes around the edges, is shown for a free-stream Mach number of 1.9. The value of $L/y_{SB}$ is seen to approach closer to the predicted value as the body becomes more nearly two dimensional. For the test with end plates (designated by $b/T \approx \infty$), the experimental value of $L/y_{SB}$ is only about 4 percent below that predicted by the continuity method. For both plane and axially symmetric bodies, the variation of $L/y_{SB}$ with nose form is less than ±10 percent of the mean experimental value.

The effect of nose form on $L/y_{SB}$ at each Mach number is similar to that noted for axially symmetric bodies, that is, the shock-location parameter tends to decrease as the nose becomes more blunt. If the differences between the value of $L/y_{SB}$ obtained with $b/T = 6.16$ are assumed to persist when $b/T \approx \infty$, then the "estimated" values shown in figure 4(b) for bodies A-1 and A-3 are obtained. These values indicate that the simplified continuity method somewhat overestimates the values of $L/y_{SB}$ obtained with two-dimensional bodies.

Effect of $b/T$ on shock form. - Shock forms obtained with body A-2 for different values of span-thickness ratio $b/T$ at $M_0$ of 1.9 are shown in figure 5. The configuration predicted for axially symmetric bodies is also shown for comparison. In this and several following figures, the common point is taken at the vertex of the detached wave and the scale factor $y_{SB}$ is the ordinate of the estimated sonic point for each body. In figure 5, the experimental shock form for low values of $b/T$ is seen to lie between the forms predicted for plane and axially symmetric flow. For $b/T = 6.16$, the

[redacted]

experimental and assumed shock forms almost coincide; whereas, for the test with end plates, the experimental wave lies slightly upstream of the predicted form beyond the shock sonic point. The small difference between the shock forms for $b/T$ of 6.16 and for the end-plate test indicates that the spillage around the ends of the model for $b/T$ of 6.16 had little effect on the shock form. The shock location, however, which is indicated by the translations of the model contour in figure 5, changes quite noticeably in the range $b/T \geq 6.16$. (See also fig. 4(b).) The transition toward the axially symmetric shock form and location as $b/T$ decreases is to be expected from the consideration that the cross-sectional area of the A-bodies approaches the cross-sectional area of axially symmetric bodies. In particular, for $b/T$ of 1.0, the configuration for the A-bodies would be expected to be very close to that obtained with the B-bodies, although some difference should persist because of the difference between the areas of a square and its inscribed circle.

Effect of body form on shock form. - The form of the detached waves obtained for each of the plane bodies with $b/T$ of 6.16 is compared with the assumed hyperbolic form in figure 6. Similar plots for the axially symmetric bodies are shown in figure 7. In figures 6(a) and 7(a), the bodies are placed at their observed location relative to the detached wave; but in figures 6(b) and 7(b), only the average location is shown because the differences in $L/y_{SB}$ were small for the bodies in these figures (table II). The theoretical sonic line is shown as a solid line between the shock and the body, and its end point on $y/y_{SB}$ of 1.0 is the theoretical location of the body sonic point relative to the shock wave.

From figures 6(a) and 7(a), the form of the body contour upstream of the sonic points is seen to have relatively little effect on the form of the detached wave, although for the plane bodies there is a noticeable trend toward less concave shock form as the nose form becomes more blunt. These variations may be important for computations of total drag based on shock form (references 7 and 8), but they are considered sufficiently small to substantiate the assumption used in the analysis of reference 1, namely, that the form of the body upstream of its sonic points has little effect on the form of the detached wave.

The contour of the body downstream of the sonic point also appears to have little effect on the shock form for the plane bodies (fig. 6(b)) but influences considerably the shape of the wave for

axially symmetric bodies (fig. 7(b)). This influence, however, is not great between the vertex of the shock wave and its sonic points. The form of the shock wave beyond its sonic points does not enter into the theory of reference 1.

An indication of the reasons for the less rapid decay of the detached waves beyond their sonic points for bodies such as B-5 and B-6 can be obtained by comparison of figures 3(g) to 3(i). (The oblique line downstream of the detached wave in the upper portion of these figures results from a scratch on the tunnel window.) For B-1 and B-3, a region of expansion is visible in the vicinity of the shoulder. The downstream portion of this expansion region diverges from the detached shock wave, so that the form of the detached wave is evidently independent of the body contour beyond the immediate vicinity of the sonic point. For B-6, however, the expansion is more gradual, so that the shock form can be influenced by a somewhat larger portion of the contour downstream of the sonic point. Similar observations for plane bodies (figs. 3(a) to 3(c)) show that expansion waves near the sonic point diverge from the detached shock wave for A-7 as well as for A-1 and A-3, so that the detached wave for A-7 should be very similar to that obtained with A-2. This expectation is confirmed in figure 6(b). These considerations indicate that near $M_0 = 1.9$, the entire detached wave can be represented to good approximation by equation (7), (appendix A) (with $y_m = 0$) when only the expansion waves that originate in the immediate vicinity of the body sonic point can reach the detached wave; for more gradually curved bodies, the detached wave beyond its sonic point may decay less rapidly than indicated by equation (7), (appendix A). In either case, however, use of the hyperbolic form to compute total drag by the methods of references 7 or 8 is unwarranted, inasmuch as small changes in shock contour can introduce considerable changes in computed drag.

Whether the hyperbola is a good approximation to the form of the detached wave at Mach numbers much higher than 1.9 remains to be established. For Mach numbers lower than 1.9, a comparison with the results of reference 2 showed that the hyperbola form is a good approximation for the detached waves ahead of cones and spheres at Mach numbers 1.17, 1.30, and 1.62. Large discrepancies appeared, however, when the shock ahead of the cones approached attachment.

Effect of angle of attack on shock form and location. - In reference 1, the shock form and location at angle of attack for two-dimensional bodies was estimated by considering separately the top and bottom halves of the configuration. The center line (see sketch, fig. 8) was taken in the free-stream direction and passed through the

[redacted]

intersection of the tangent lines from the body sonic points. The sonic-point ordinates $y_{SB,1}$ and $y_{SB,2}$ are measured from the center line and determine the relative scale of the top and bottom halves of the configuration. According to reference 1, the values of $y_S/y_{SB}$ for each half should be the same, so that shock form, shock location, and drag coefficient should have the same values as for symmetrical two-dimensional bodies.

In figure 8, the shock waves agree well with the predicted form for the two extreme noses A-1 and A-3 at angle of attack. For each body, the shock forms are almost identical at zero angle of attack and 6.5° angle of attack. By superposition of schlieren negatives, this result was found to hold also for the axially symmetric bodies; that is, the detached wave at angle of attack for each body was almost identical in form to the detached wave at zero angle of attack. When the two shock waves were superimposed, the relative position of the bodies was approximately that obtained by rotating one of the bodies about the center of the line joining its estimated sonic points. In effect, the detached wave therefore remained almost stationary as the body was rotated through a range of angles of attack.

In plotting figure 8, different scale factors ($y_{SB,1}$ and $y_{SB,2}$) were used for the upper and lower portions of the configurations so that the agreement with the predicted configuration could be established. This difference in scale factors results in a slight discontinuity at the center line of A-1 at angle of attack. This discontinuity can be eliminated and the experimentally observed configuration can be obtained by multiplying the ordinate and the abscissa of the lower half by the ratio $y_{SB,2}/y_{SB,1}$, which was 1.07 for an angle of attack of 6.5°. The value of $L/y_{SB}$ at 6.5° angle of attack was found to be 1.99 for both halves of body A-1 and 2.11 for both halves of body A-3. These values are slightly higher than those obtained at zero angle of attack (1.95 and 2.07, respectively).

Pressure distributions. - The distribution of pressure coefficient over the nose of each model investigated in the 18- by 18-inch tunnel is shown in figures 9 and 10. For each body, the location of the experimental sonic point at zero angle of attack is also shown, together with the estimated location. The local Mach number on the surface was related to the local pressure coefficient by

$$M^2 = \frac{2}{\gamma-1}\left\{\left[\frac{P_0}{P_n}\frac{p_0}{P_0}\left(1+\frac{\gamma}{2}M_0{}^2 C_p\right)\right]^{\frac{1-\gamma}{\gamma}} - 1\right\} \qquad (1)$$

[redacted]

where $P_n$ is the stagnation pressure behind a normal shock occurring at the free-stream Mach number. Equation (1) is obtained with the assumptions that the stagnation streamline passes close to the normal element of the detached wave and that the stagnation pressure beyond the shock is not noticeably affected by viscosity. For a free-stream Mach number of 1.9, equation (1) becomes

$$M^2 = 5 \left[ 1.597 \left(1 + 2.527\, C_p\right)^{-0.2857} - 1 \right] \qquad (1a)$$

where

$$C_p = 0.3957 \left( \frac{p}{p_0} - 1 \right) \qquad (2)$$

The relation given by equation (1a) is plotted in figure 11, from which the pressure coefficient corresponding to sonic velocity is seen to be 0.68.

In figures 9 and 10, the actual sonic point is seen to occur upstream of the estimated location for most of the bodies and coincides with the estimated location for the others. The estimated location, however, corresponds to the maximum constriction, or shoulder, which happens to coincide with the sonic point in the one-dimensional analogy used throughout the analysis of reference 1. The actual sonic point, as pointed out in reference 9, should be located somewhat upstream of this shoulder.

The pressure distributions in figures 9 and 10 show that the displacement of the curves at angle of attack from those for zero angle of attack is in general less upstream of the sonic point than downstream of it, although for the pointed bodies (figs. 9(c) and 10(c)) a strong expansion appears near the tip at negative angles of attack. This region of strong expansion near the vertex is visible in figure 3(e).

For bodies A-1, A-2, A-3, A-4, B-1, B-2, and B-3, expansion to negative pressure coefficients occurred near the shoulder, with subsequent recompression. For bodies A-5, A-6, A-7, B-4, B-5, and B-6 (figs. 9(e) to 9(g), and 10(d) to 10(f)), the expansion near the shoulder at zero angle of attack does not reach negative pressure coefficients but is nevertheless sufficient to indicate that the expansion waves that originate a short distance downstream of the shoulder and beyond will reach the detached wave only at large distances from the vertex.

The pressure coefficients some distance downstream of the shoulder are compared with theoretical pressure coefficients of wedges or cones with half-angles equal to the inclination of the straight portions of the blunt bodies in figures 9(e), 9(f), 10(d), and 10(e). For the plane bodies (A-5 and A-6), the actual pressures at a distance $x/t$ of 1.0 from the vertex are found to be considerably lower than the corresponding wedge pressures; whereas, for the axially symmetric bodies (B-4 and B-5) the pressures approach closer to the corresponding cone pressures. These figures show how blunt bodies, if correctly designed, may have lower drags than pointed bodies of the same thickness ratio or length-to-diameter ratio. If the region of underpressure (relative to the corresponding pointed body) is sufficiently large to more than counteract the effect of the region of overpressure near the vertex, lower drag can be attained with a blunt body. As will be pointed out subsequently, of the bodies tested, only B-5 attained a total drag lower than that of the corresponding cone.

The effect of finite span on the pressure distribution along the center line for the A-bodies was negligible for the portion of the contour upstream of the shoulder (fig. 9(b)). This result is somewhat surprising in view of the large effect of $b/T$ on shock location. The difference is probably due to the fact that shock location depends on conditions along the entire span; whereas the effect of the edges on pressure distribution is greatest near the ends and decreases as the center line is approached. Downstream of the shoulder, the pressure coefficient for body A-2 approached zero slightly more rapidly when end plates were attached (fig. 9(b)). This result indicates that the pressure coefficients for the other plane bodies may also have approached their asymptotic values more rapidly if they were truly two-dimensional.

Drag coefficients. - From figures 9 and 10, the drag coefficients for each model were obtained by numerical integration of the pressure coefficients plotted against $y/t$ and $y/R$. These drag coefficients are presented in table III. The coefficient $\left(C_D\right)_{total}$ is based on the maximum cross-sectional area of each model and is defined as

$$\left(C_D\right)_{total} = \sum_{0}^{1} C_p \, \Delta (y/t) \quad \text{(plane bodies)} \qquad (3)$$

[redacted]

or

$$\left(C_D\right)_{total} = 2\sum_{0}^{1} C_p(y/R)\Delta(y/R) \quad \text{(axially symmetric bodies)} \quad (3a)$$

The coefficient $\left(C_D\right)_{SB}$ is the drag coefficient for the portion of each body upstream of its estimated sonic points and is defined as

$$\left(C_D\right)_{SB} = (t/y)_{SB} \sum_{0}^{(y/t)_{SB}} C_p\Delta(y/t) \quad \text{(plane bodies)} \quad (4)$$

or

$$\left(C_D\right)_{SB} = 2(R/y)_{SB}^2 \sum_{0}^{(y/R)_{SB}} C_p(y/R)\Delta(y/R) \quad \text{(axially symmetric bodies)} \quad (4a)$$

Theoretically predicted values of $\left(C_D\right)_{SB}$ are also shown in table III for comparison. For the A-bodies, the experimental values of $\left(C_D\right)_{SB}$ range from 1.11 to 1.28; for the B-group, the values vary from 1.07 to 1.13. The assumption that the form of the nose has little effect on the drag upstream of the sonic point is thus seen to be more valid for axially symmetric than for plane bodies. If the bluntest of the plane bodies, A-1, is ignored, however, the values of $\left(C_D\right)_{SB}$ for the remaining nose forms are found to lie within 5 percent of the mean value. Hence, except for extremely blunt bodies, the aforementioned assumption can probably be considered valid as an approximation for plane as well as axially symmetric bodies at a Mach number of 1.9.

Comparison of the mean experimental values (1.20 for plane bodies and 1.11 for axially symmetric bodies) with predicted values shows that the predicted values are almost the reverse of the experimental values; that is, the predicted value for axially symmetric bodies is close to the mean experimental value for plane bodies, and vice versa. Most of this discrepancy can probably be attributed to the oversimplification of conditions near the sonic line used in reference 1. Small changes in the assumed inclination of the sonic line, for example, can entirely eliminate the discrepancy. Thus, if

in equation (11) (appendix A) the value of $\eta$ is reduced from 30° to 26°, $(C_D)_{SB}$ decreases from 1.21 to 1.12. This sensitivity of drag to the assumed conditions at the sonic line indicates that a much more detailed analysis of the flow field is necessary if an accuracy greater than that shown in table III is required.



Comparison of the total drag coefficients for the blunt bodies with those of wedges and cones (table III) shows that all blunt bodies except B-5 had higher total drag than the corresponding pointed bodies. It is evident that the high-pressure portion of the blunt body must be quite small relative to the entire body if its drag is to be less than that of a pointed body of the same thickness ratio. For thin bodies, theory indicates that the blunting required for a minimum-drag contour is almost invisible (reference 10).

Nose inlets. - For the axially symmetric nose-inlet configurations shown in figures 3(m) to 3(p), the location of the detached shock wave relative to the inlet lip was used to estimate the mass spillage from equations (4a) and (1a). (The procedure used to measure L is given in appendix B.) From the resulting values of $y_m/y_{SB}$, the shock form relative to the inlet was calculated from equations (7) and (8a) of appendix A. The assumed and experimental shock forms for these inlets are shown in figure 12, and the values of $\tau$ obtained from shock location and from other data are given in table IV. The other data for the configurations of figures 12(a) and 12(b) consisted of measurements of stagnation pressure in the combustion chamber and area at the outlet, where sonic velocity was reached. Inasmuch as the flow coefficient of the outlet could only be roughly estimated, the resulting values of $\tau$ obtained from data at the outlet may be rather inaccurate. In particular, in figure 12(a), although the outlet was supposedly completely closed, some leakage was believed to have occurred; the value obtained from shock location may therefore be more correct than the value obtained from the nominal outlet area.

In table IV, the value of $\tau$ of 0.40 for the inlet of figure 12(c) was obtained from an examination of the negative of the schlieren photograph shown in figure 3(o), in which the slip streamline originating at the intersection of the oblique shock with the detached wave could be clearly seen. Because this slip streamline passed close to the lip of the inlet, an estimate of $y_m$ was easily obtained. In figure 12(d), the outlet of the diffuser was completely closed, and the value of $\tau$ was estimated from the number of perforations in the inlet. The flow coefficient for these perforations was assumed to be 0.50, which has been found to agree reasonably well with experimental results (reference 6).

The agreement between predicted values and actual values of $\tau$ appears to be good. The experimental and assumed shock forms also agree fairly well except in figure 12(c), where interaction with the oblique shock from the nose occurs. Although none of the detached waves is precisely normal at $y = y_m$, the assumption that the detached wave is an hyperbola with origin at $y = y_m$ leads to fairly accurate values of $\tau$. A procedure for improving the accuracy is discussed in appendix B.

## SUMMARY OF RESULTS

An investigation of shock form, shock location, and drag for a variety of plane and axially symmetric bodies that produce detached shock waves was conducted. The shock location was obtained for a range of Mach numbers from 1.8 to 2.9, and the shock form and drag were obtained at a Mach number of 1.9. The results of this investigation may be summarized as follows:

1. The form of the detached wave between its sonic points at a Mach number of 1.9 was represented to good approximation for all bodies by an hyperbola asymptotic to the free-stream Mach lines. For most bodies, this hyperbola was also a good approximation for the portion of the detached shock wave downstream of its sonic points. The relative independence of the shock form beyond its sonic points of the form of the body downstream of its sonic point appears to be due to the overexpansion that generally occurs in the vicinity of the body sonic point, so that characteristics from only a small portion of the body contour near the sonic point reach the detached wave.

2. The variation of the shock-location parameter with nose form was less than ±10 percent of the mean value over the Mach number range investigated. For the axially symmetric bodies, the experimental values of shock-location parameter fell between the values predicted by the geometric method and those predicted by the one-dimensional continuity method. For plane bodies with finite span, the experimental values of shock-location parameter were considerably lower than predicted values. This result was attributed to spillage of air around the ends of these models. Evidence was obtained that experimental values approached the predicted values when the end effects were reduced.

3. For both plane and axially symmetric bodies, the variation of shock location and shock form with angle of attack was small.

4. At a Mach number of 1.9, the drag coefficient for the portion of each body upstream of its sonic points varied from 1.07 to 1.13 for axially symmetric nose forms and from 1.11 to 1.28 for plane nose forms. The predicted value was 6 percent lower than the mean experimental value for plane bodies and 9 percent higher than the mean experimental value for axially symmetric bodies.

5. The spillage of air outside the cowl of several nose inlets as predicted from shock location agreed well with the spillage estimated by other means. A method was given for improving the accuracy of the mass-flow computation by use of the actual rather than the hyperbolic shock form.

Lewis Flight Propulsion Laboratory,
National Advisory Committee for Aeronautics,
Cleveland, Ohio.

[redacted]

## APPENDIX A

## RÉSUMÉ OF THEORY

The simplified representation used in reference 1 for the flow pattern associated with detached shock waves is shown in figure 1. The shock wave form between its vertex and its sonic point is assumed to be represented by an hyperbola asymptotic to the free-stream Mach waves and the sonic line is assumed to be straight and inclined normal to the arithmetic mean of the stream directions at the sonic points S and SB. The location of the sonic point on the body SB was estimated by application of the method suggested by Busemann (reference 9). This estimate locates SB at the point of tangency of the body with a line inclined at the wedge or cone half-angle for which the shock becomes detached. For plane bodies, this detachment angle $\lambda_d$ has almost the same value as the stream angle at the shock sonic point $\lambda_S$ so that the inclination of the sonic line $\eta$ was assumed to be

$$\eta = \frac{1}{2}(\lambda_S + \lambda_d) \cong \lambda_S \tag{5}$$

For axially symmetric bodies, the value of $\eta$ was given by

$$\eta = \frac{1}{2}(\lambda_S + \theta_d) \tag{5a}$$

The representations that correspond to these assumptions are shown in figure 1(a) for closed-nose bodies and in figure 1(b) for open-nose bodies (nose inlets). The two representations become identical when $y_m = 0$, that is, when no air enters the inlet. The maximum mass flow into the inlet occurs when the shock is attached to the lip, that is, when $y_m = y_{SB}$. The fraction of this maximum that spills over the cowl is seen to be, for two-dimensional inlets,

$$\tau = 1 - \frac{y_m}{y_{SB}} \tag{6}$$

and, for axially symmetric inlets,

$$\tau = 1 - \left(\frac{y_m}{y_{SB}}\right)^2 \tag{6a}$$

[redacted]

In order to represent the assumed hyperbolic form of the detached shock wave, the following equation was used in reference 1:

$$\beta\left(\frac{y}{y_{SB}} - \frac{y_m}{y_{SB}}\right) = \sqrt{\left(\frac{x}{y_{SB}}\right)^2 - \left(\frac{x_0}{y_{SB}}\right)^2} \tag{7}$$

where

$$\frac{x_0}{y_{SB}} = \beta\sqrt{\beta^2 \tan^2 \varphi_S - 1}\left(\frac{y_S}{y_{SB}} - \frac{y_m}{y_{SB}}\right)$$

and where $y_m$ is zero for closed bodies. Application of the one-dimensional continuity equation to the simplified configurations yielded the following expressions for $y_S/y_{SB}$:

for two-dimensional bodies,

$$\frac{y_S}{y_{SB}} = \frac{1 - \frac{y_m}{y_{SB}} B \cos \lambda_S}{1 - B \cos \lambda_S} \tag{8}$$

and, for axially symmetric bodies,

$$\frac{y_S}{y_{SB}} = \sqrt{\frac{1 - \left(\frac{y_m}{y_{SB}}\right)^2 B \cos \eta}{1 - B \cos \eta}} \tag{8a}$$

where the stagnation pressure ratio $(P_s/P_0)_c$, which occurs in the quantity B, is evaluated at the shock wave on the streamline that represents the centroid of the mass flow crossing the sonic line.

The assumptions made in reference 1 led to the selection of the ratio $L/y_{SB}$ as a logical shock-location parameter, where L is the distance in the free-stream direction between the vertex of the detached wave and the sonic point on the body and $y_{SB}$ is the ordinate of the estimated body sonic point (fig. 1). In the approximate theory of reference 1, this parameter is independent of the form of the body and depends only on the free-stream Mach number and the

flow spillage. The equations obtained for this parameter by application of the one-dimensional continuity relation were, for two-dimensional flow,

$$\frac{L}{y_{SB}} = \left(1 - \frac{y_m}{y_{SB}}\right)\left(\frac{C + B \sin \lambda_S}{1 - B \cos \lambda_S}\right) \tag{9}$$

and, for axially symmetric flow,

$$\frac{L}{y_{SB}} = \sqrt{\frac{1 - \left(\frac{y_m}{y_{SB}}\right)^2 B \cos \eta}{1 - B \cos \eta}} (C + \tan \eta) - C \frac{y_m}{y_{SB}} - \tan \eta \tag{9a}$$

Another expression for $L/y_{SB}$ resulted directly from the assumption that the form of the nose upstream of its sonic points does not appreciably affect the form or the location of the detached wave or the sonic line. This expression, which was called the geometric approximation, was given as

$$\frac{L}{y_{SB}} = \cot \delta_d \tag{10}$$

where $\delta_d$ is the wedge or cone half-angle corresponding to shock detachment for the given free-stream Mach number. Equation (10) was expected to yield an upper limit of the shock location parameter, whereas equations 9 and 9(a) were expected to yield an average value of the parameter for a wide variety of nose forms.

The drag coefficient for the portion of closed bodies upstream of their sonic points was estimated by an application of the momentum equation to the representation of figure 1(a). The following equation for this coefficient was obtained for both plane and axially symmetric bodies:

$$\left(C_D\right)_{SB} = 2\left(\frac{1 - kB \cos \eta}{1 - B \cos \eta}\right) \tag{11}$$

[redacted]

This coefficient is based on the cross-sectional area of the body at its estimated sonic point. The experimental investigation reported herein was designed primarily to check the validity of equations (7) to (11).



[redacted]

## APPENDIX B

## MEASUREMENT OF L AND IMPROVEMENT OF ACCURACY IN PREDICTION OF MASS SPILLAGE FOR NOSE INLETS

Measurement of L. - For some inlets, particularly for those with projecting central bodies, the detached wave may be far from normal at $y_m$. A consistent method of measuring $L/y_{SB}$ for such cases is indicated in figure 13. Inasmuch as the shock location when $y_m = 0$ is given approximately by $L/y_{SB} = \cot \theta_d$, and $L/y_{SB} = 0$ when $y_m = y_{SB}$, it appears reasonable to measure L at the intersection of the shock with the line tangent to the lip and inclined at the angle $\theta_d$. This procedure is consistent with the concepts of reference 1 and gives directly an approximate value of $y_m/y_{SB}$ as a function of $L/y_{SB}$. A better approximation, however, is obtained by using the value of $L/y_{SB}$ measured by this method in the equation derived from the continuity method (equation (9a)). The procedure illustrated in figure 13 was used to measure L in figures 3(m), 3(n), and 3(p), as well as in figure 3(o), inasmuch as the detached wave was not precisely normal to the free stream at $y = y_m$ for any of these inlets.

Improvement in accuracy of predicting $\tau$. - The assumption that the detached wave is hyperbolic with origin at $y = y_m$ may in some cases be a poor approximation. This assumption, however, is nonessential to the method. If the form of the detached wave is known from photographs, the location of the sonic point on the shock is easily determined. A straight line from this point to the lip of the inlet should then be a good approximation to the sonic line. If the flow area at this sonic line is known, the flow area in the free stream can be calculated directly from the one-dimensional continuity equation. Consequently, $y_m$ can be obtained directly from the actual form of the detached wave. The mean stagnation-pressure ratio required in this computation can be chosen as in reference 1 or from the mean shock angle between $y = y_m$ and $y = y_s$. The results presented in this report, however, indicate that variations in the form of the detached wave do not greatly affect the computed values of $\tau$, so that in most cases equation (9a) should be adequate for establishing an approximate relation between $\tau$ and $L/y_{SB}$. If the oblique shock from a central body intersects the detached wave above $y = y_m$, however, the use of the actual shock form is probably advisable.

[redacted]

## REFERENCES

1. Moeckel, W. E.: Approximate Method for Predicting Form and Location of Detached Shock Waves Ahead of Plane and Axially Symmetric Bodies. NACA TN 1921, 1949.

2. Heberle, Juergen W., Wood, George P., and Gooderum, Paul B.: Data on Shape and Location of Detached Shock Waves on Cones and Spheres. NACA TN 2000, 1950.

3. Evvard, John C., and Wyatt, DeMarquis D.: Investigation of a Variable Mach Number Supersonic Tunnel with Nonintersecting Characteristics. NACA RM E8J13, 1948.

4. Wyatt, DeMarquis D., and Hunczak, Henry R.: An investigation of Convergent-Divergent Diffusers at Mach Number 1.85. NACA RM E6K21, 1947.

5. Moeckel, W. E., Connors, J. F., and Schroeder, A. H.: Investigation of Shock Diffusers at Mach Number 1.85. II - Projecting Double-Shock Cones. NACA RM E6L13, 1947.

6. Hunczak, Henry R., and Kremzier, Emil J.: Characteristics of Perforated Diffusers at Free-Stream Mach Number 1.90. NACA RM E50B02, 1950.

7. Ferri, Antonio: Method for Evaluating from Shadow or Schlieren Photographs the Pressure Drag in Two-Dimensional or Axially Symmetrical Flow Phenomena with Detached Shock. NACA TN 1808, 1949.

8. Munk, M. M., and Crown, J. C.: The Head Shock Wave. Memo. 9773, Naval Ord. Lab. (Silver Spring, Md.), Aug. 25, 1948.

9. Busemann, Adolf: A Review of Analytical Methods for the Treatment of Flow with Detached Shocks. NACA TN 1858, 1949.

10. de Kármán, Th.: The Problem of Resistance in Compressible Fluids. Quinto Convegno "Volta", Reale Accademia d'Italia (Roma), Sett. 30-Ott. 6, 1935, pp. 3-57.

[redacted]

TABLE I - COORDINATES FOR BODIES A-7 AND B-6

| x | y | |
|---|---|---|
| | A-7 | B-6 |
| 0 | 0 | 0 |
| .25 | .58 | .59 |
| .50 | .75 | .81 |
| .75 | .84 | .98 |
| 1.00 | .92 | 1.13 |
| 1.50 | 1.04 | 1.37 |
| 2.00 | 1.12 | 1.57 |
| 3.00 | 1.21 | 1.85 |
| 4.00 | 1.25 | 2.07 |
| 5.00 | 1.25 | 2.23 |
| 6.00 | 1.25 | 2.37 |
| 7.00 | 1.25 | 2.50 |

NACA

TABLE II - SHOCK-LOCATION PARAMETERS OBTAINED IN 18- by 18-INCH TUNNEL

[Free-stream Mach number, 1.9.]

| Body | b/T | $L/y_{SB}$ | |
|---|---|---|---|
| | | Experimental | Predicted |
| A-1 | 6.16 | 1.97 | |
| A-2 | 4.62 | 1.93 | |
| A-2 | 6.16 | 2.04 | |
| A-3 | 6.16 | 2.08 | |
| A-4 | 6.16 | 2.01 | |
| A-5 | 4.00 | 1.98 | |
| A-6 | 4.00 | 2.04 | |
| A-7 | 4.00 | 2.04 | |
| A-2 | $\approx \infty$ | 2.23 | 2.31 |
| B-1 | | 0.90 | 0.925 |
| B-2 | | .97 | |
| B-3 | | 1.00 | |
| B-4 | | 1.00 | |
| B-5 | | .97 | |
| B-6 | | 1.00 | |

[redacted]

TABLE III - COMPARISON OF THEORETICAL AND EXPERIMENTAL DRAG COEFFICIENTS

[Free-stream Mach number, 1.9.]

| Body | $(C_D)_{total}$ | $C_{D,SB}$ | |
|---|---|---|---|
| | | Experimental | Predicted |
| A-1 | 1.24 | 1.28 | 1.12 |
| A-2 | 1.11 | 1.20 | |
| A-3 | 1.11 | 1.21 | |
| A-4 | 1.07 | 1.11 | |
| A-5 | .72 [a](0.205) | 1.17 | |
| A-6 | .82 [a]( .51) | 1.15 | |
| A-7 | .77 | 1.21 | |
| B-1 | 0.96 | 1.09 | 1.21 |
| B-2 | .77 | 1.11 | |
| B-3 | .76 | 1.07 | |
| B-4 | .27 [a](0.21) | 1.13 | |
| B-5 | .64 [a]( .68) | 1.13 | |
| B-6 | .28 | 1.09 | |

[a]Coefficients for wedges or cones with half-angle equal to the inclination of the straight portion of the corresponding blunt bodies.

TABLE IV - VALUES OF $\tau$ FOR CONFIGURATIONS OF FIGURE 12


| Figure | $\tau$ | |
|---|---|---|
| | From shock location | From other data |
| 12(a) | 0.93 | ~1.00 |
| 12(b) | .54 | .55 |
| 12(c) | .38 | .40 |
| 12(d) | .58 | .59 |

[redacted]

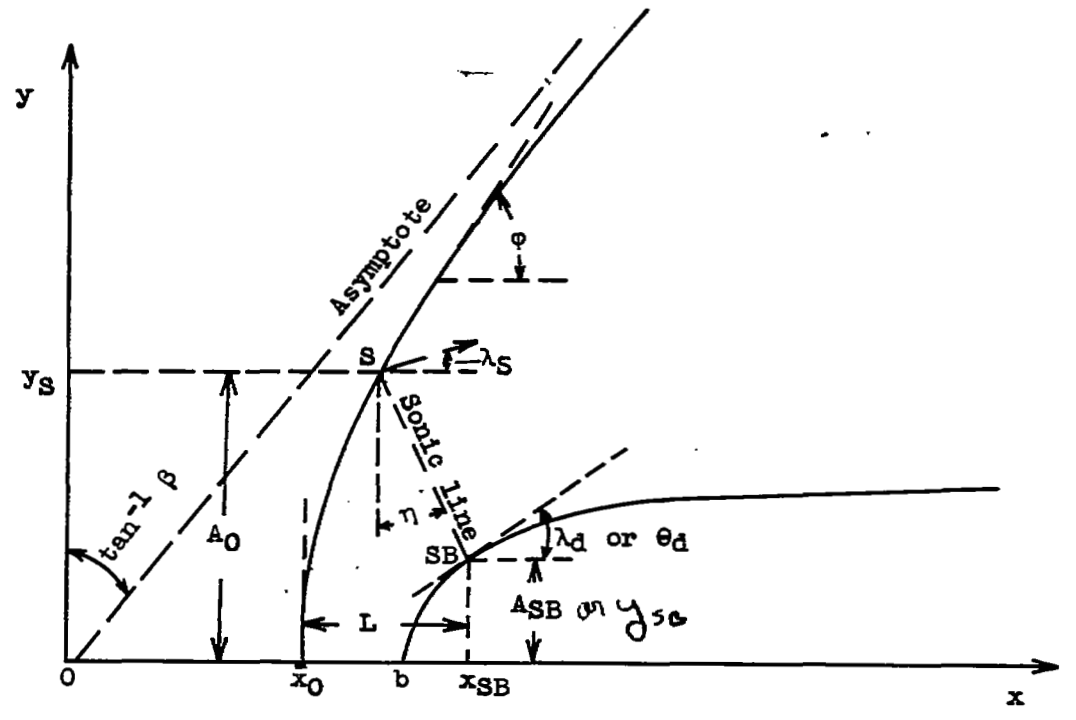


(a) Closed-nose bodies.

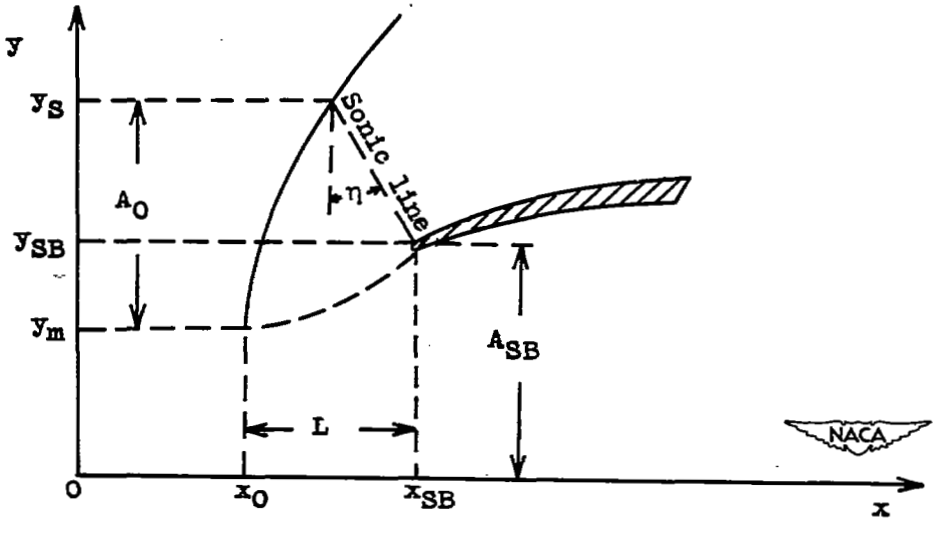


(b) Open-nose bodies with spillage.

Figure 1. - Simplified representations of flow with detached shock waves (reference 1).

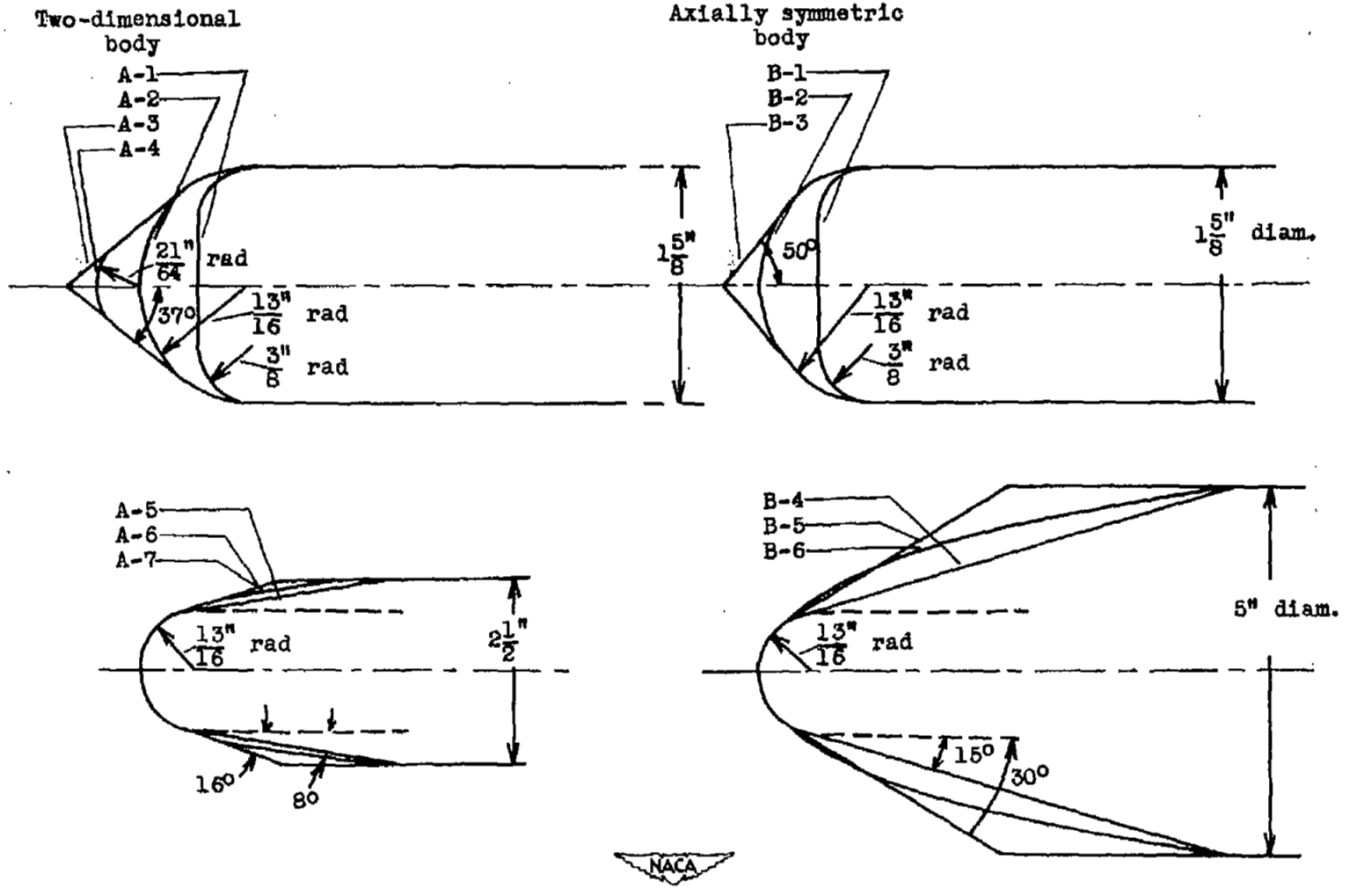


Figure 2. - Sketches of bodies investigated at free-stream Mach number of 1.9. For variable Mach number tunnel investigation, these bodies were reduced to 0.5-inch maximum thickness or diameter.

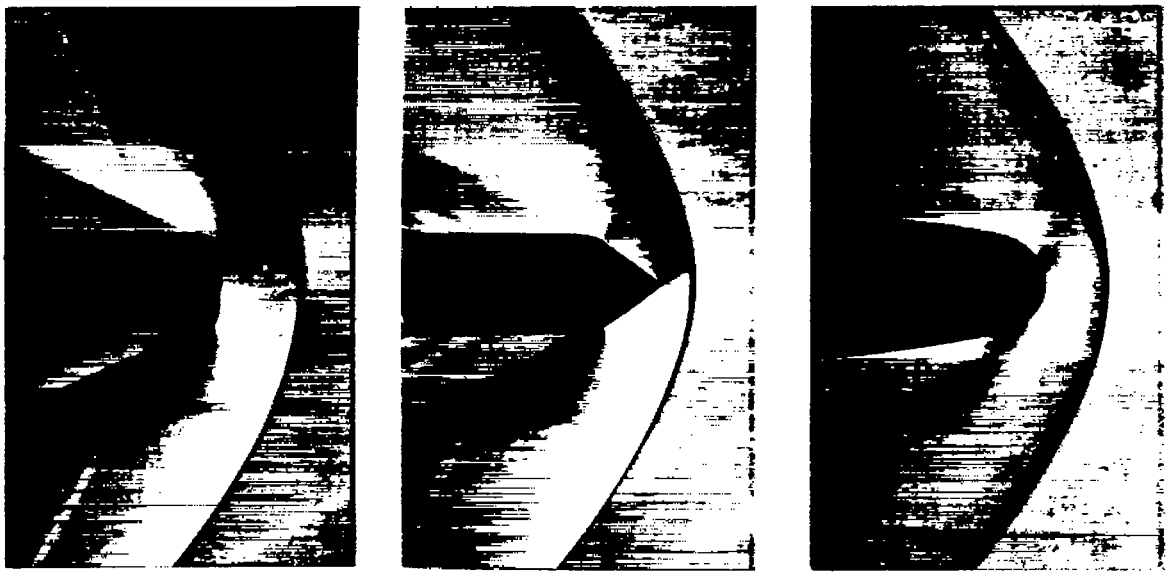

(a) Body A-1; angle of attack, 0°.

(b) Body A-3; angle of attack, 0°.

(c) Body A-7; angle of attack, 0°.

(d) Body A-1; angle of attack, 5.7°.

(e) Body A-3; angle of attack, 5.7°.

(f) Body A-7; angle of attack, 5.9°.

NACA

C-25505
3-30-50

Figure 3. - Typical detached-shock configurations at free-stream Mach number of 1.9.

(g) Body B-1; angle of attack, 0°.

(h) Body B-3; angle of attack, 0°.

(i) Body B-6; angle of attack, 0°.

(j) Body B-1; angle of attack, 8°.

(k) Body B-3; angle of attack, 8°.

(l) Body B-6; angle of attack, 8°.

NACA
C-25506
3-30-50

Figure 3. - Continued. Typical detached-shock configurations at free-stream Mach number of 1.9.

[redacted]

(m) Convergent-divergent inlet (reference 4).

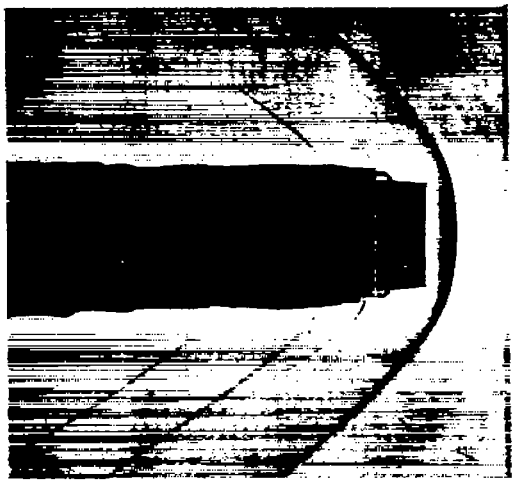

(n) Convergent-divergent inlet (reference 4).

(o) Double-shock cone inlet (reference 5).

(p) Perforated inlet (reference 6).

NACA
C-25504
3-30-50

Figure 3. - Concluded. Typical detached-shock configurations at free-stream Mach number of 1.9.

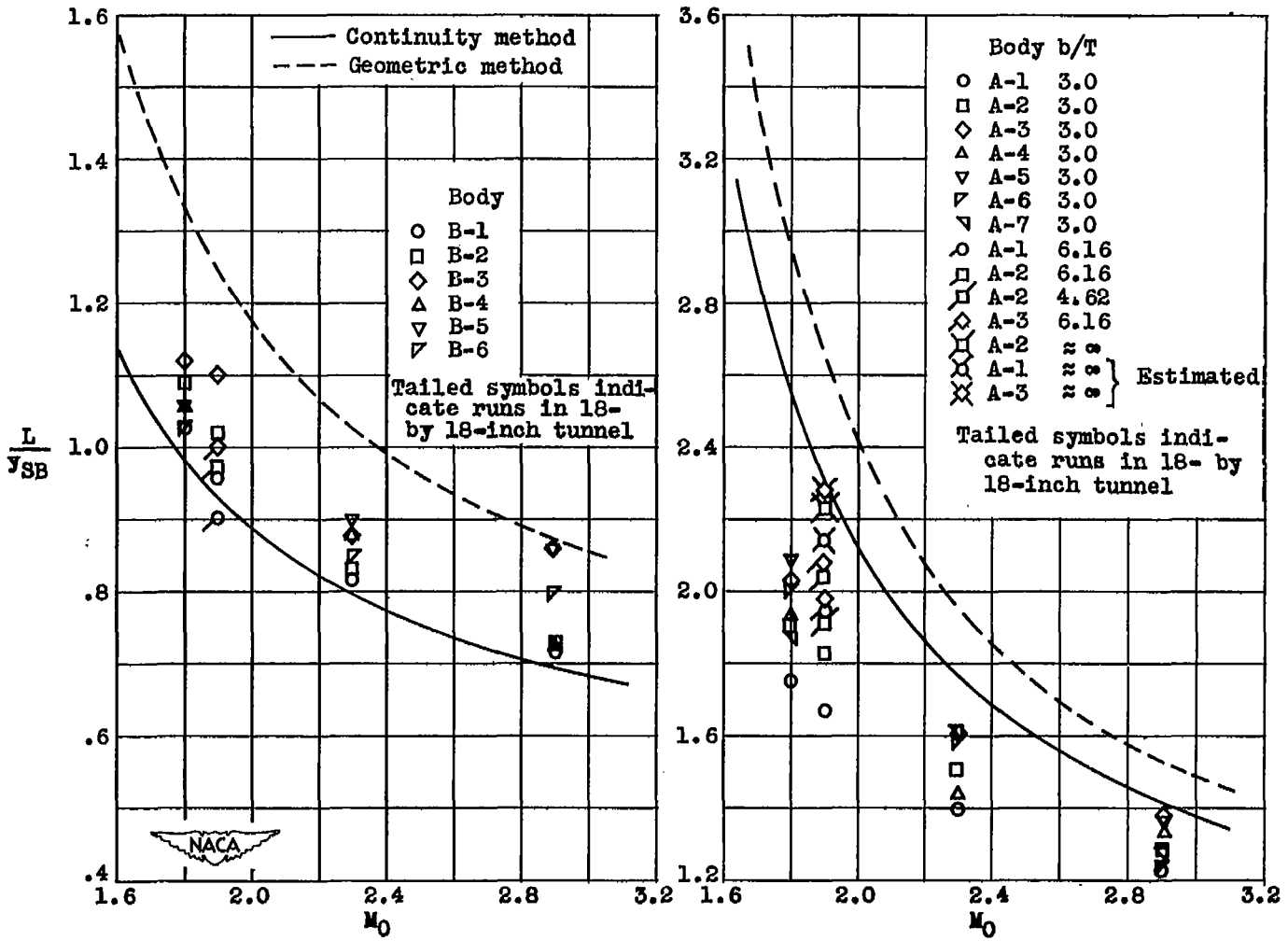


(a) Axially symmetric bodies.

(b) Two-dimensional bodies.

Figure 4. - Experimental and theoretical variation of shock-location parameter with free-stream Mach number.

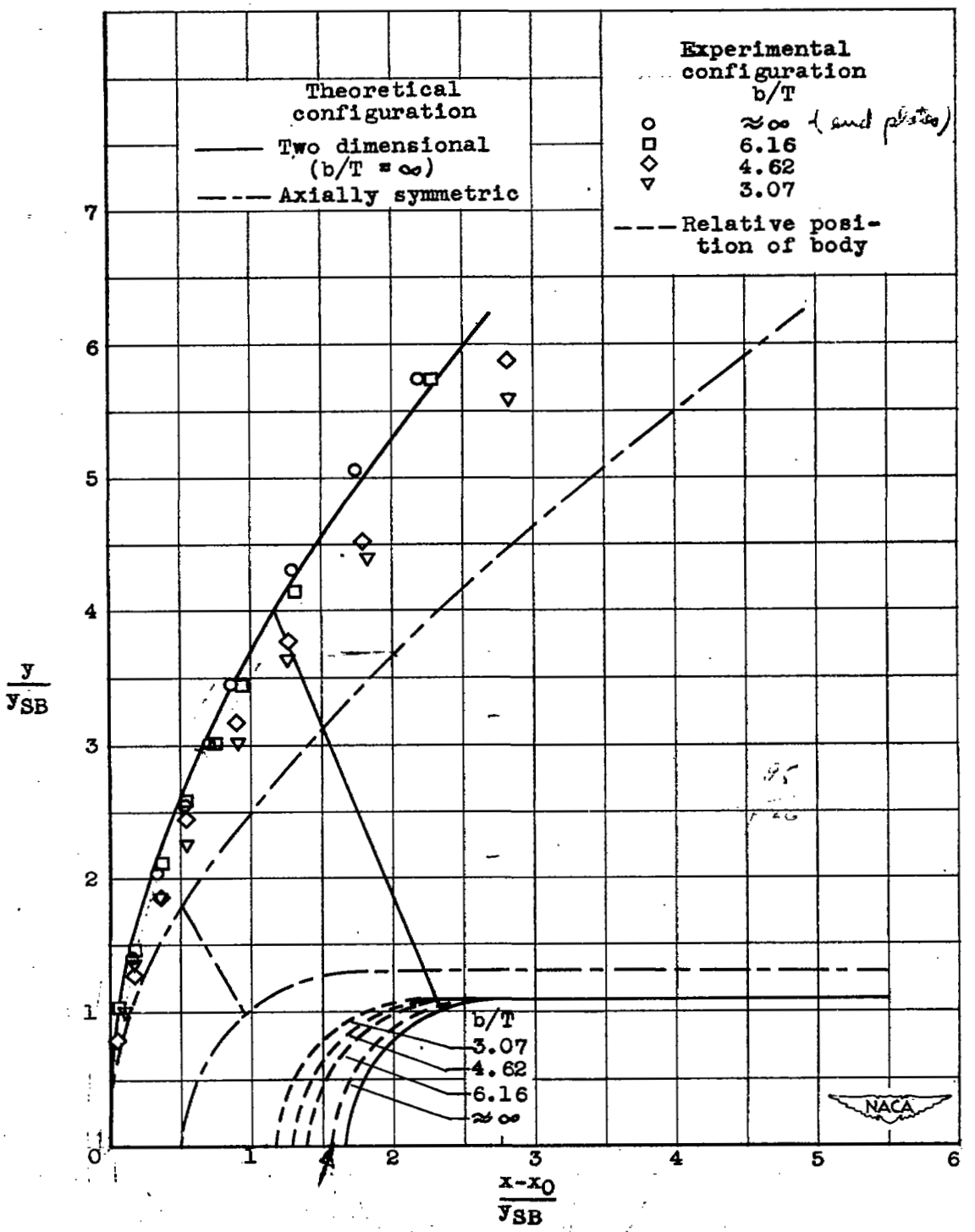


Figure 5. - Effect of span-thickness ratio on shock form. Body A-2; free-stream Mach number, 1.9.

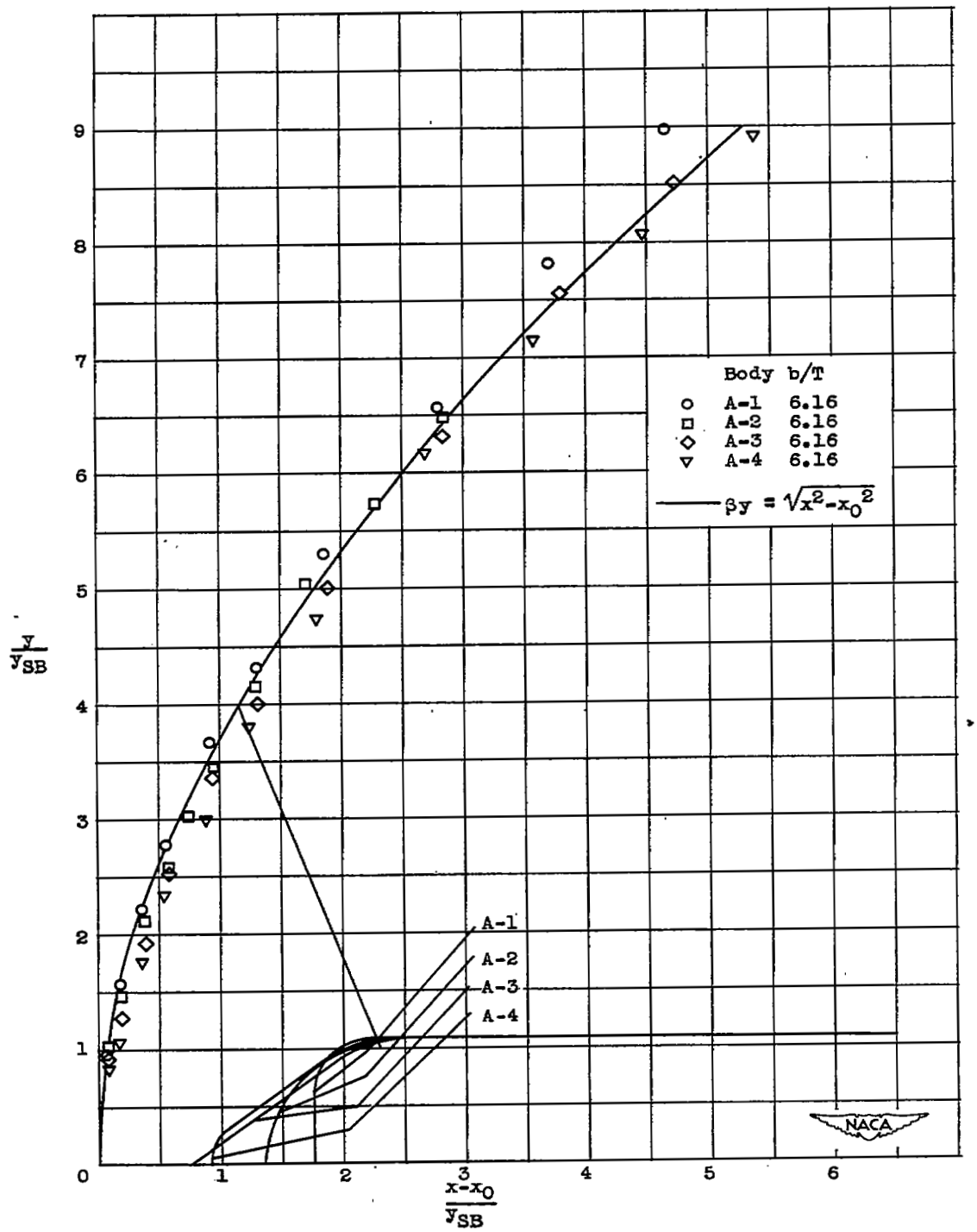


(a) Body form variable upstream of estimated sonic point.

Figure 6. - Effect of two-dimensional body form on shock form. Free-stream Mach number, 1.9.

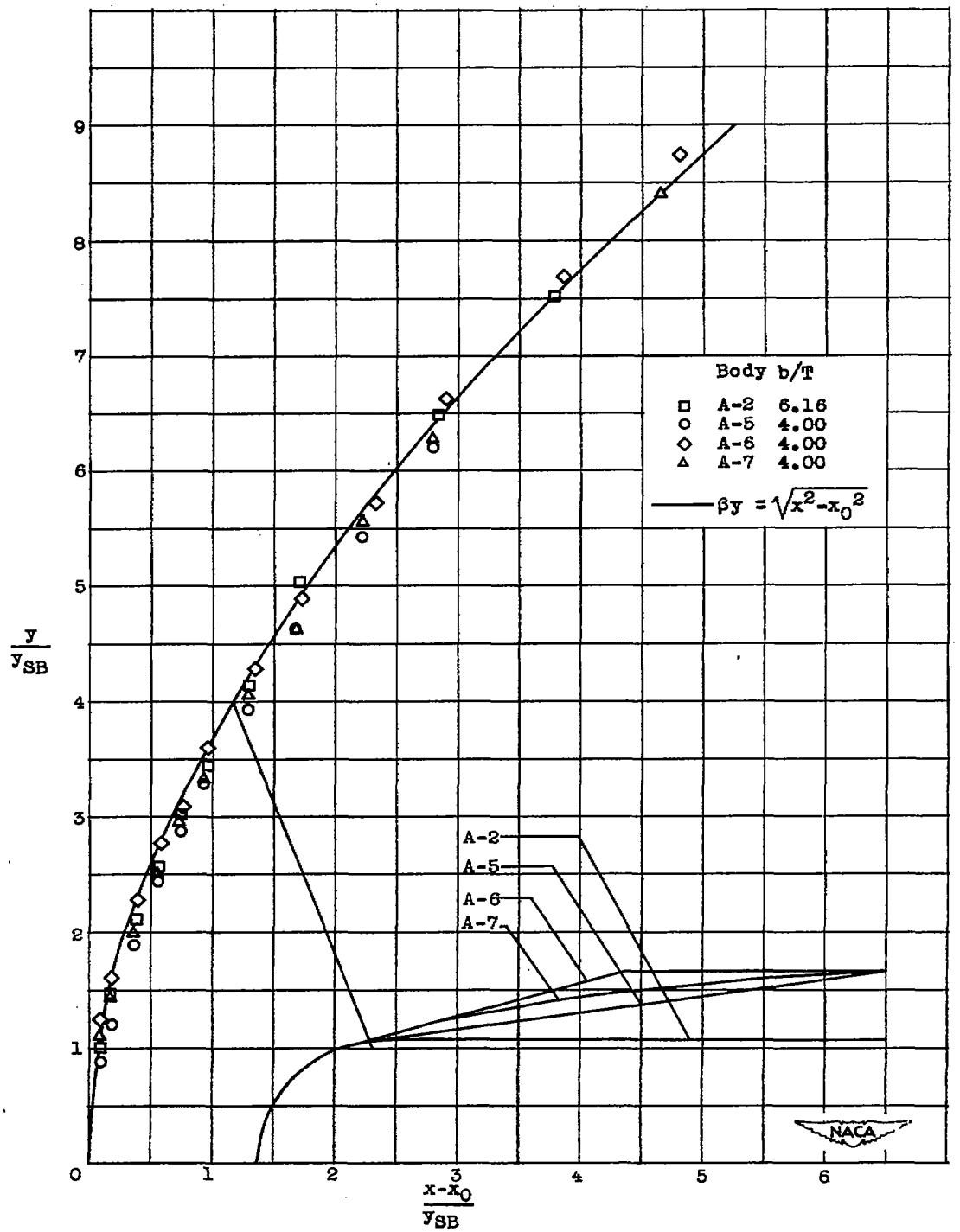


(b) Body form variable downstream of estimated sonic point.

Figure 6. - Concluded. Effect of two-dimensional body form on shock form. Free-stream Mach number, 1.9.

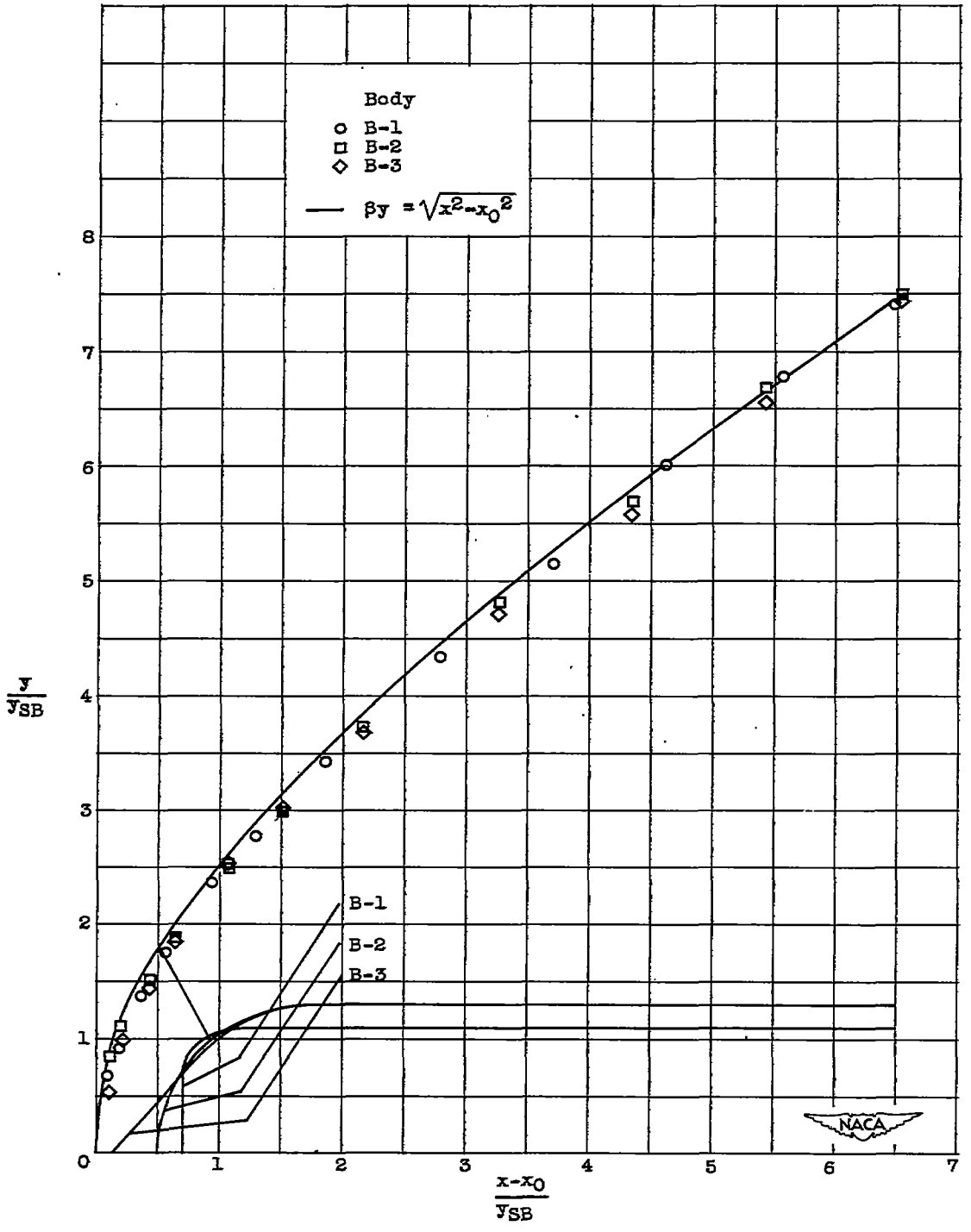


(a) Body form variable upstream of estimated sonic point.

Figure 7. - Effect of axially symmetric body form on shock form. Free-stream Mach number, 1.9.

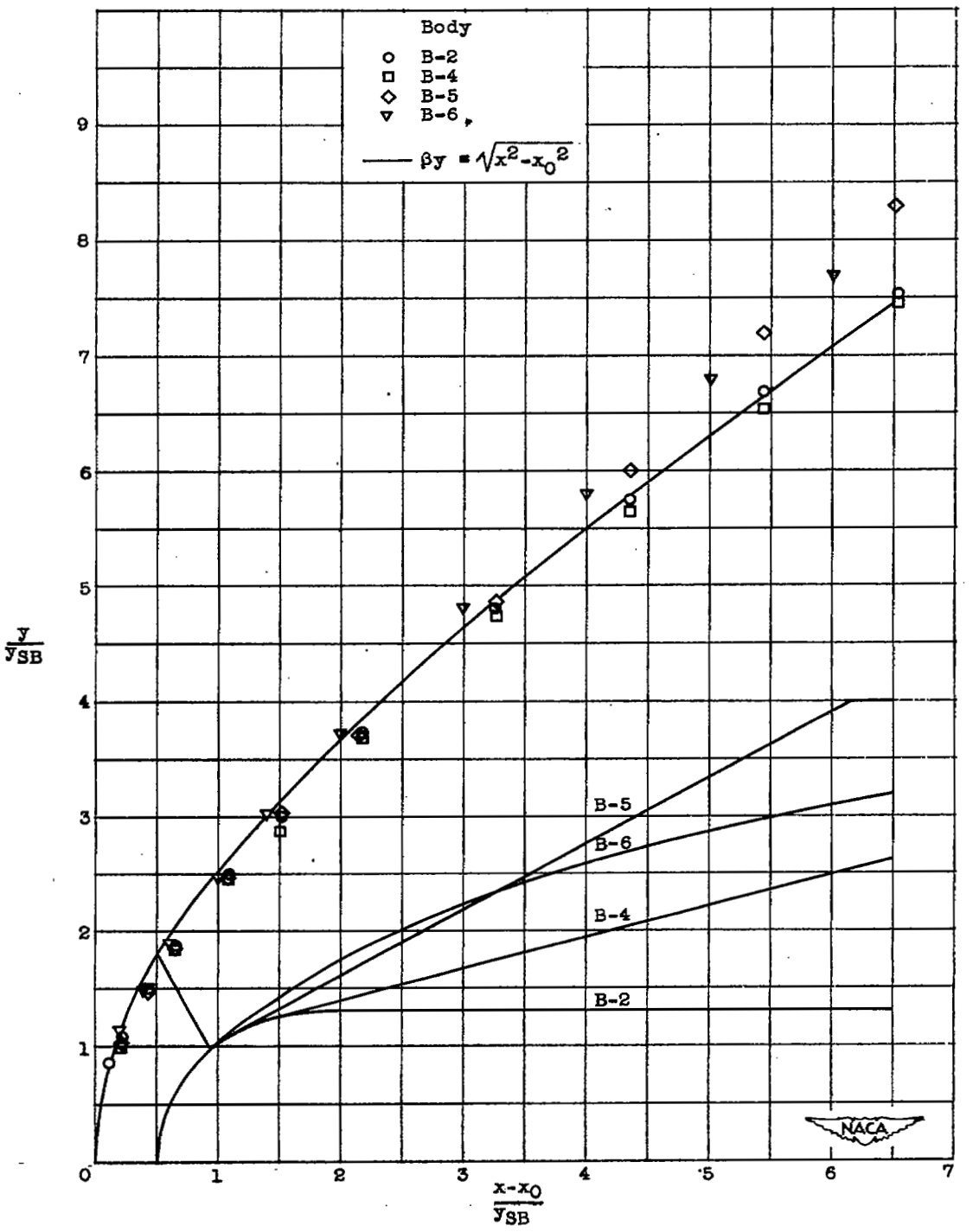


(b) Body form variable downstream of estimated sonic point.

Figure 7. - Concluded. Effect of axially symmetric body form on shock form. Free-stream Mach number, 1.9.

[redacted]

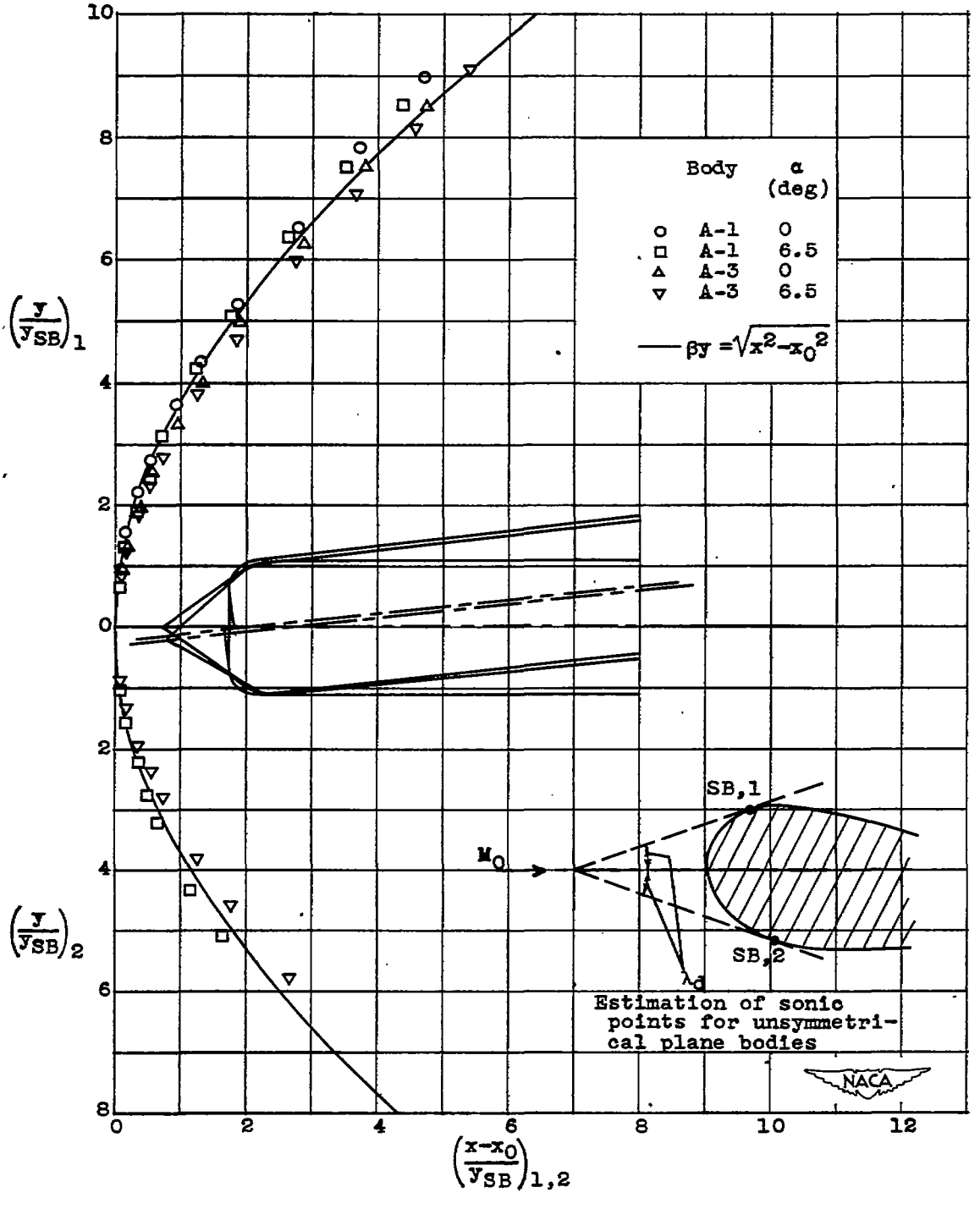


Figure 8. - Effect of angle of attack on shock form and location. Free-stream Mach number, 1.9.

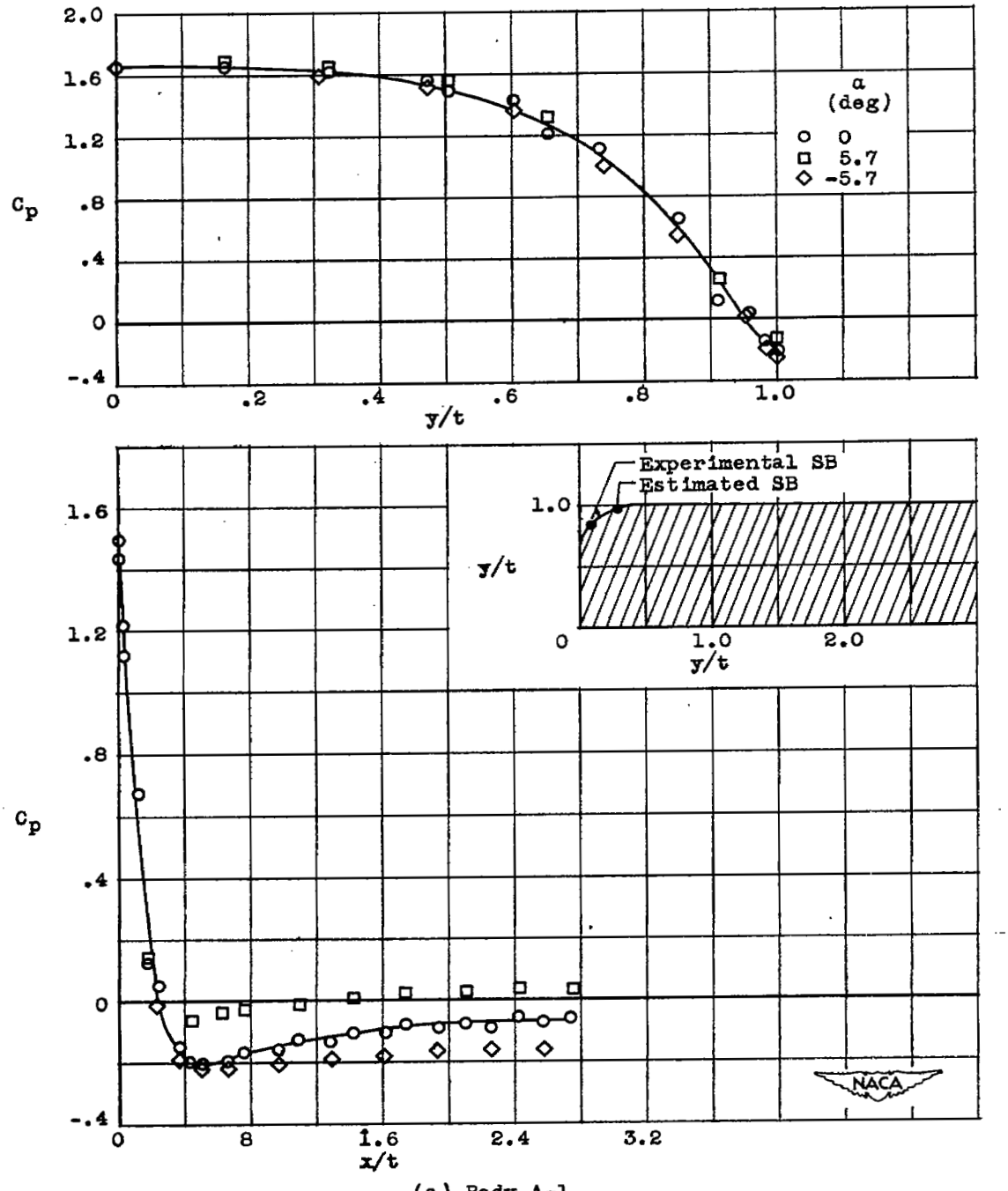


(a) Body A-1.

Figure 9. - Pressure distribution over two-dimensional bodies. Free-stream Mach number, 1.9.

[redacted]

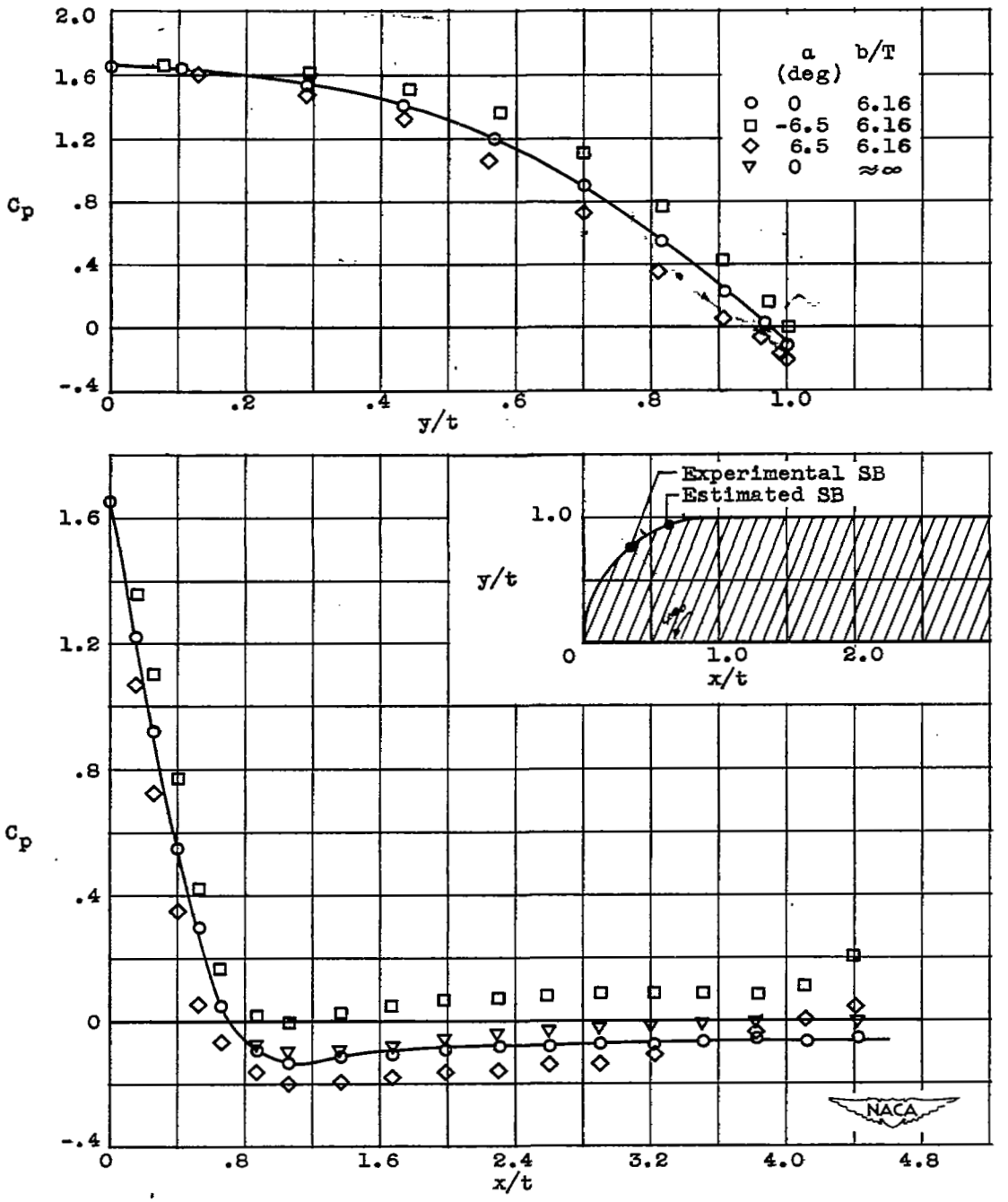


(b) Body A-2.

Figure 9. - Continued. Pressure distribution over two-dimensional bodies. Free-stream Mach number, 1.9.

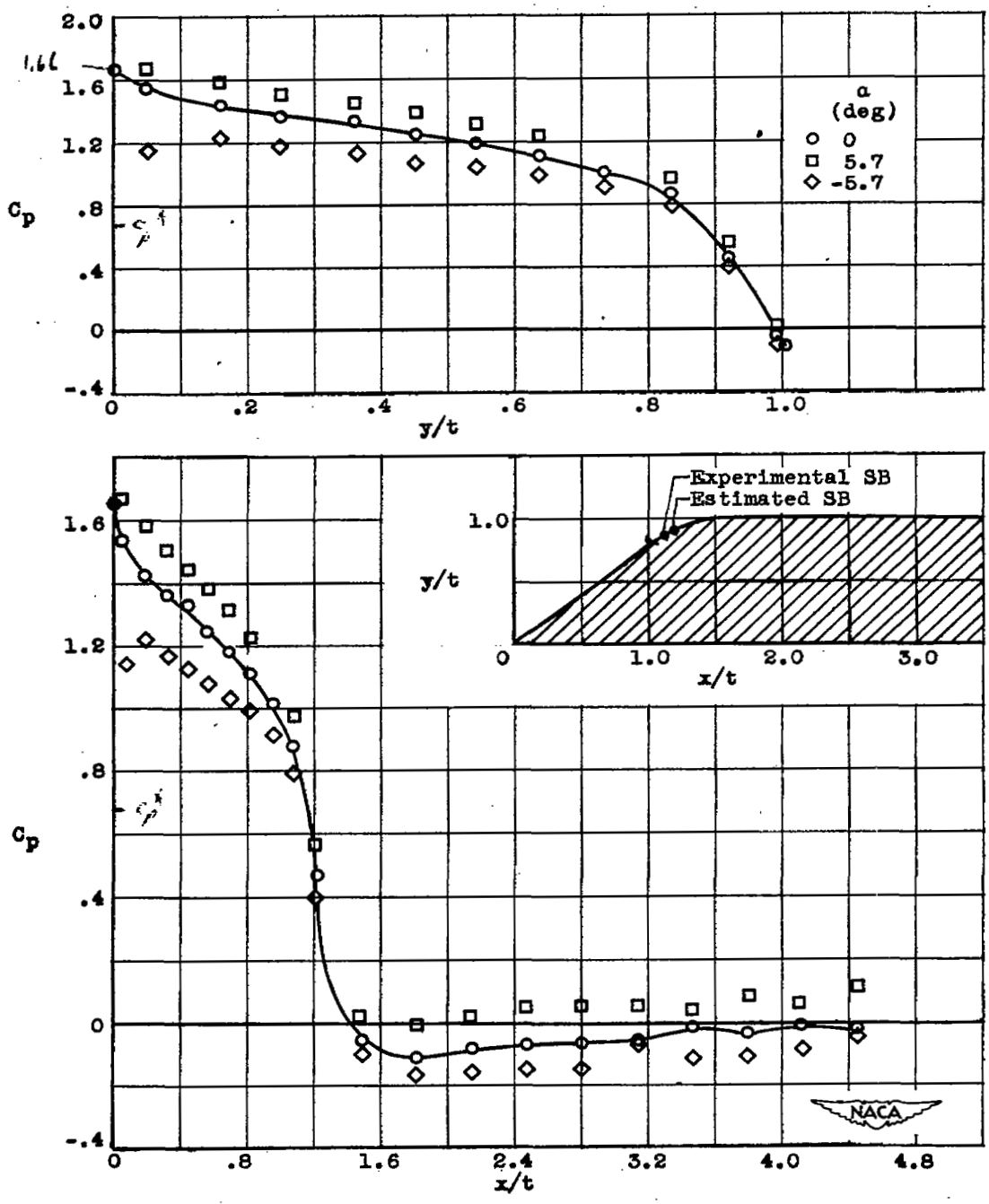


(c) Body A-3.

Figure 9. - Continued. Pressure distribution over two-dimensional bodies. Free-stream Mach number, 1.9.



[redacted]

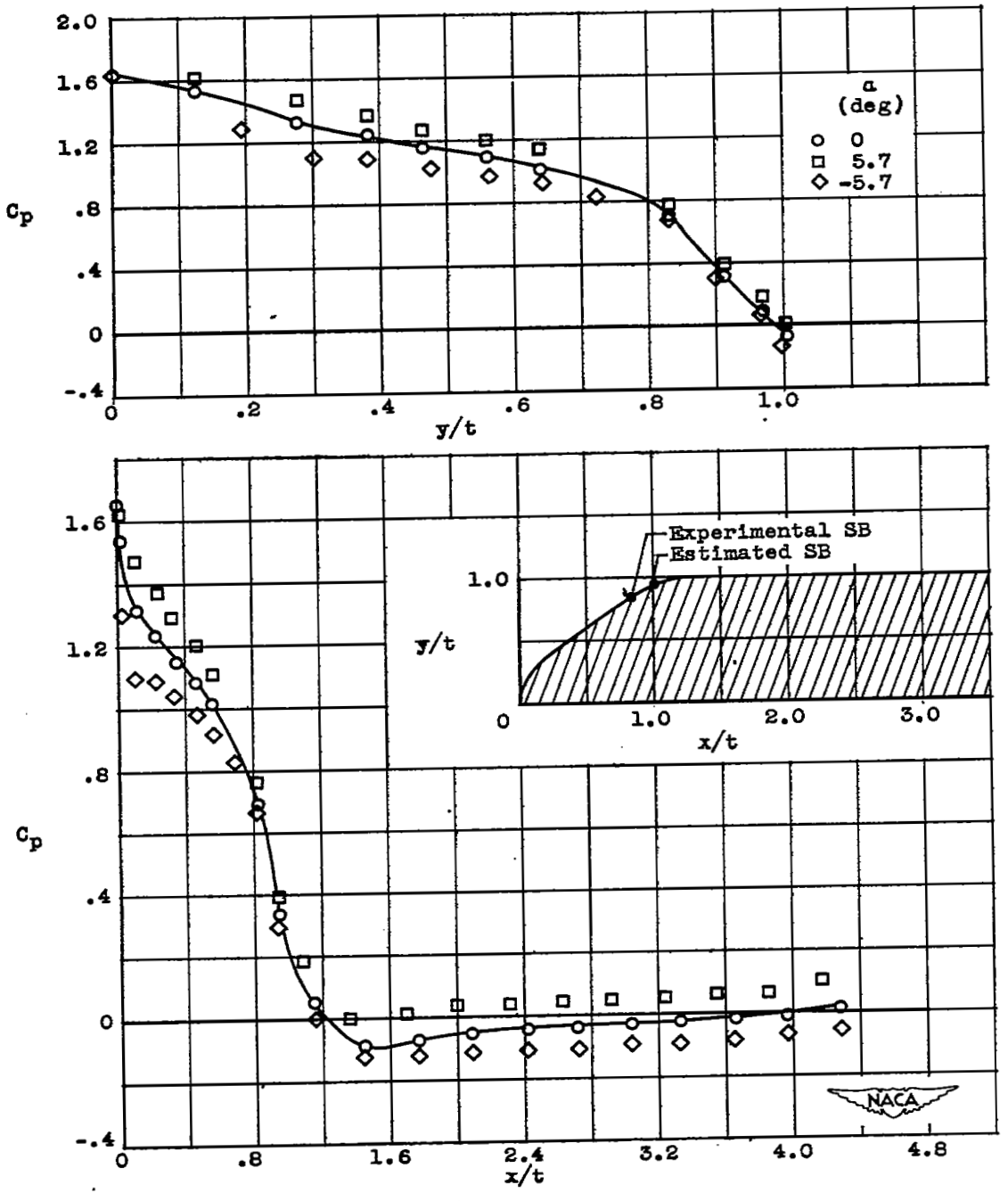


(d) Body A-4.

Figure 9. - Continued. Pressure distribution over two-dimensional bodies. Free-stream Mach number, 1.9.

[redacted]

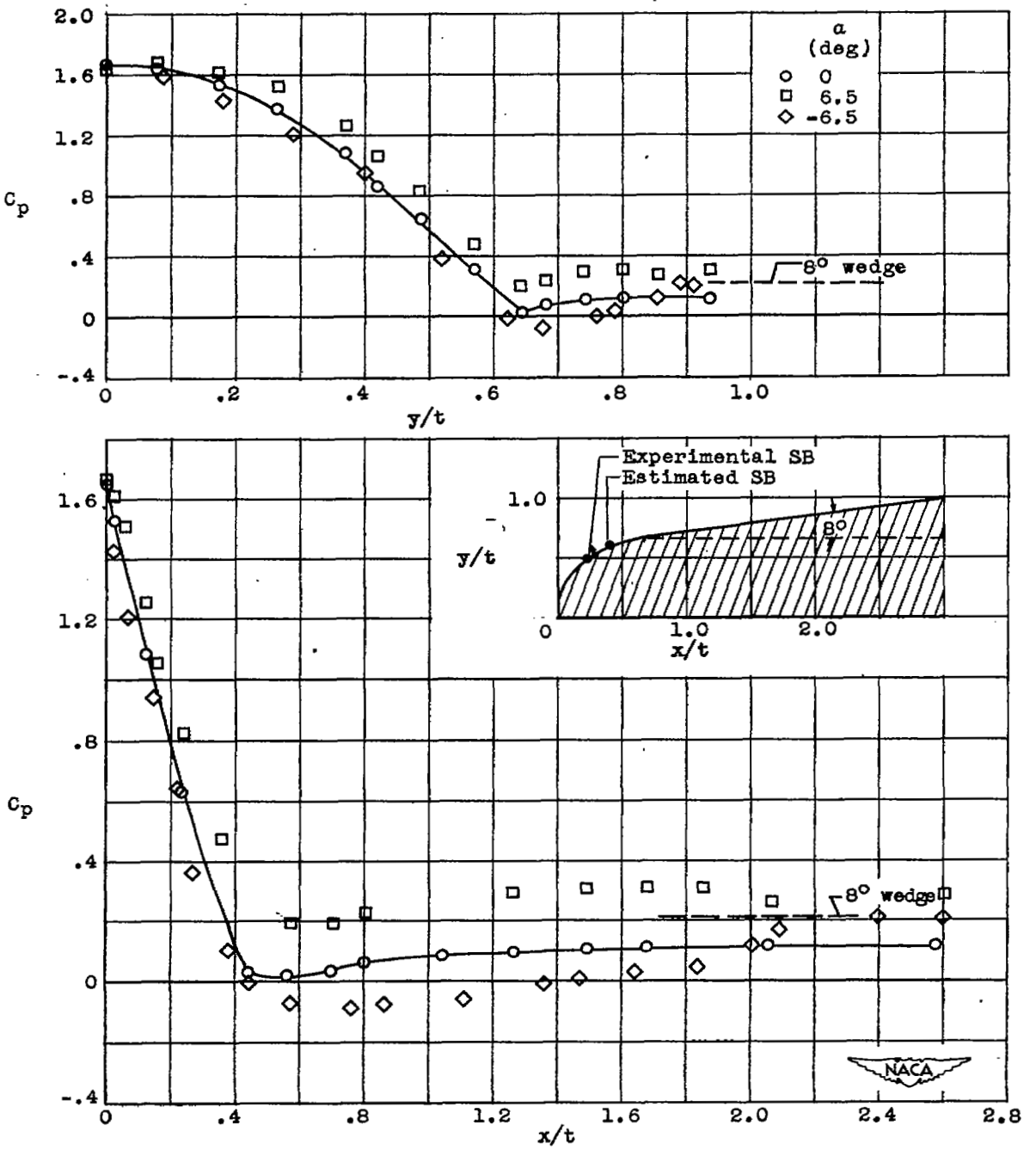


(e) Body A-5.

Figure 9. - Continued. Pressure distribution over two-dimensional bodies. Free-stream Mach number, 1.9.

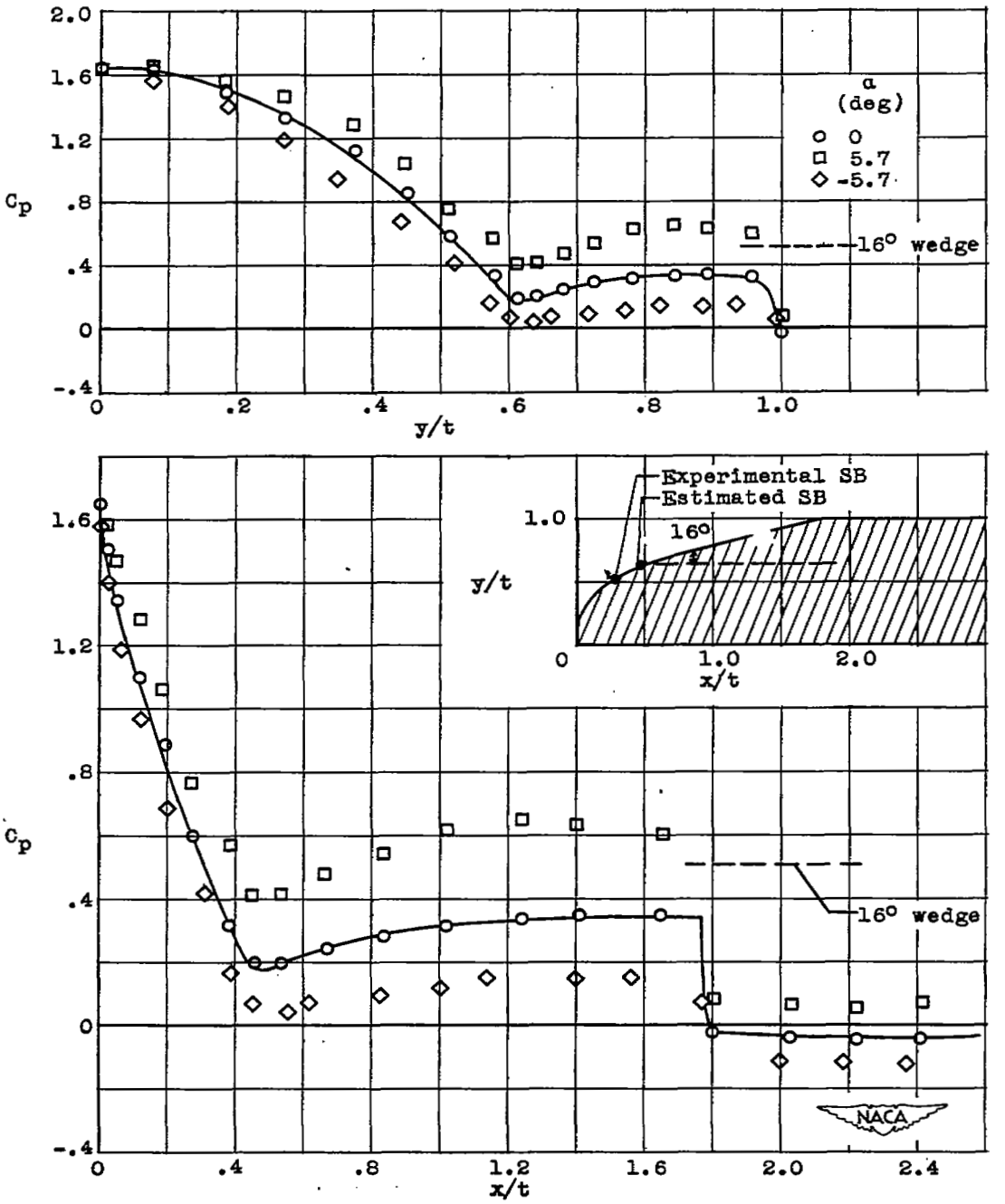


(f) Body A-6.

Figure 9. - Continued. Pressure distribution over two-dimensional bodies. Free-stream Mach number, 1.9.

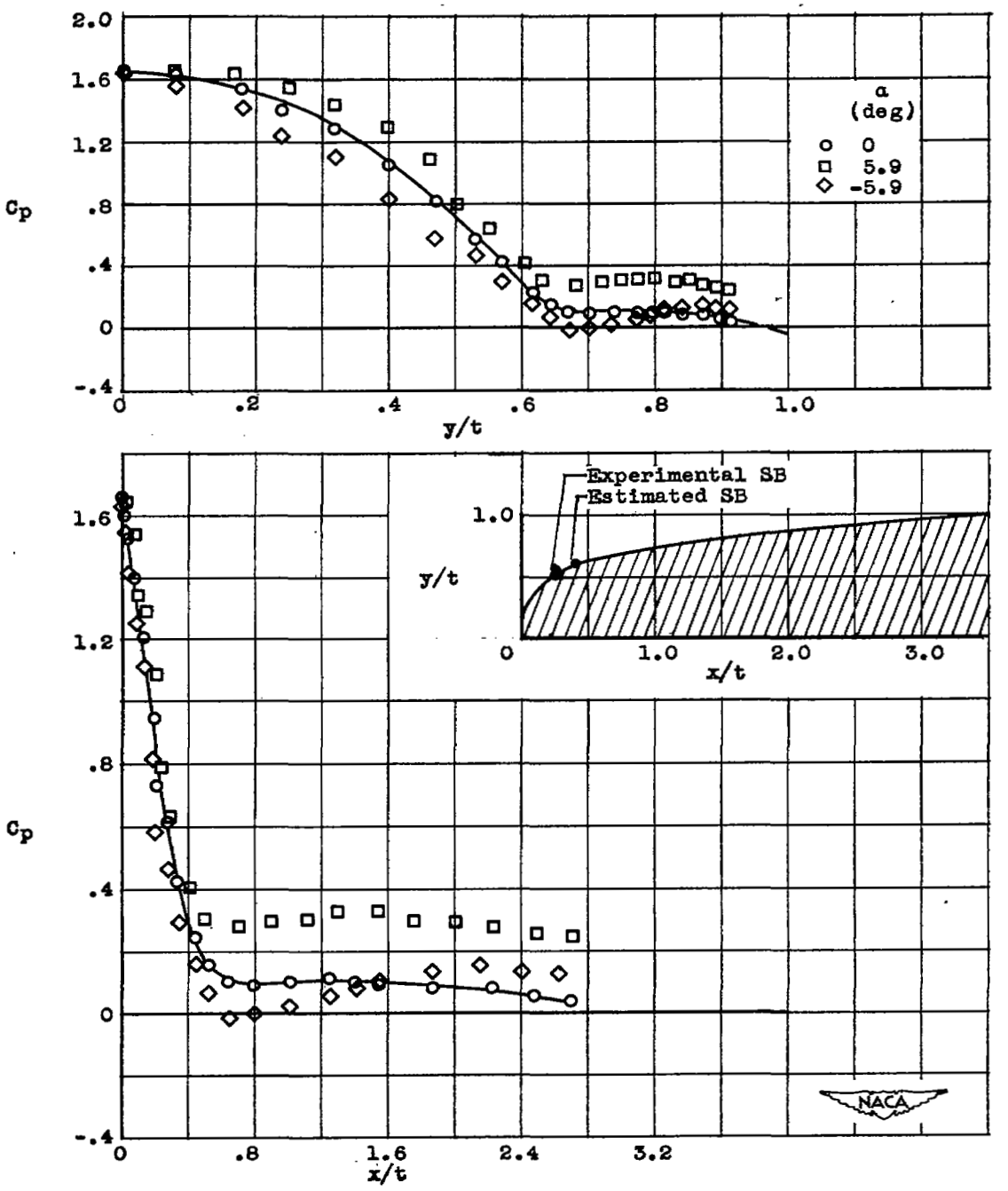


(g) Body A-7.

Figure 9. - Concluded. Pressure distribution over two-dimensional bodies. Free-stream Mach number, 1.9.

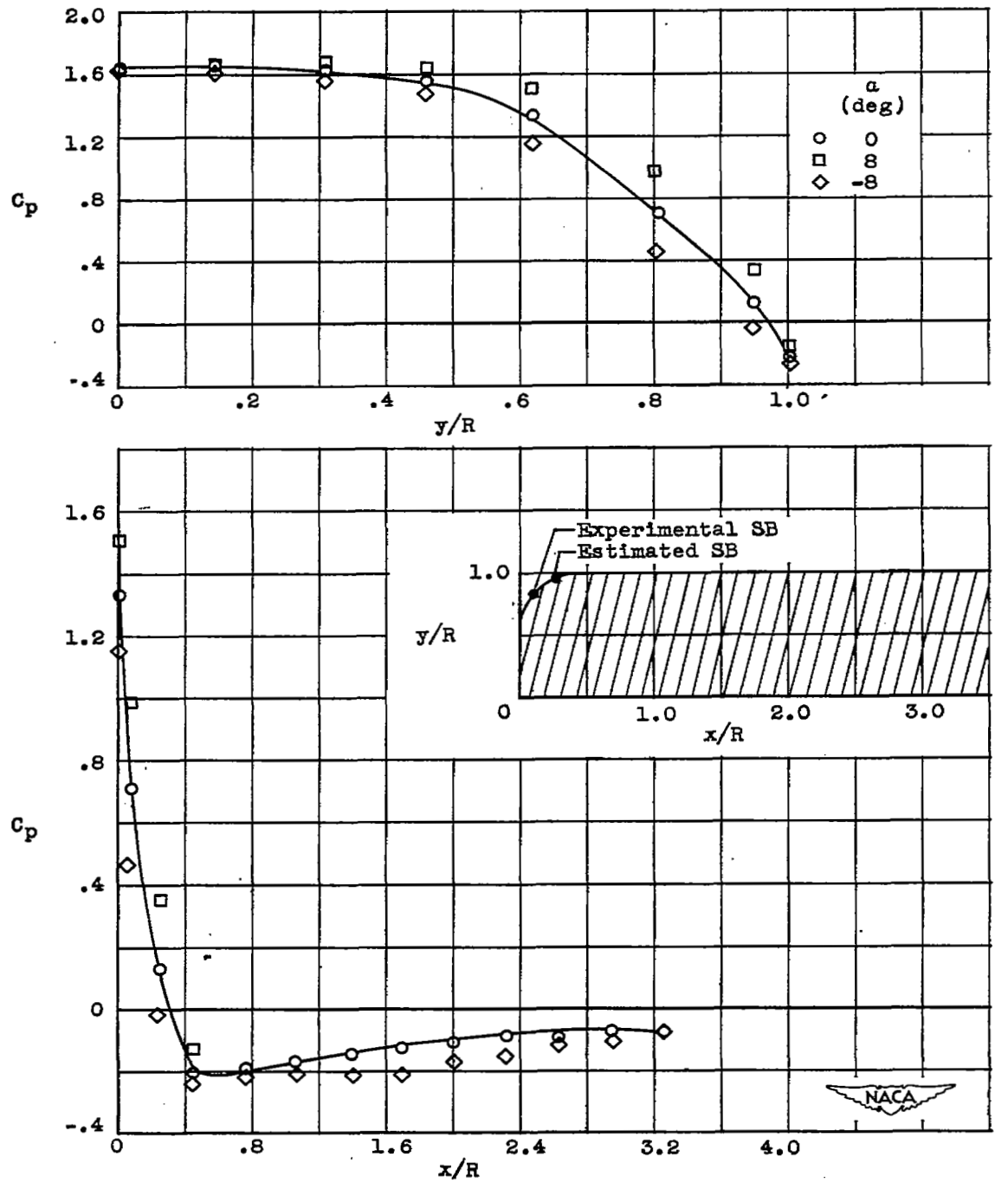


(a) Body B-1.

Figure 10. - Pressure distribution over axially symmetric bodies. Free-stream Mach number, 1.9.

[redacted]

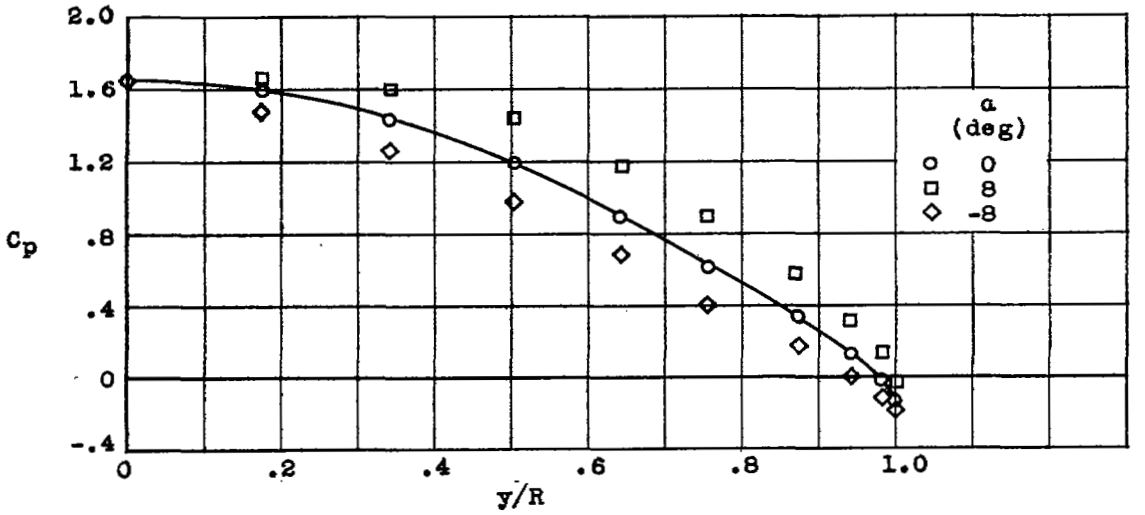


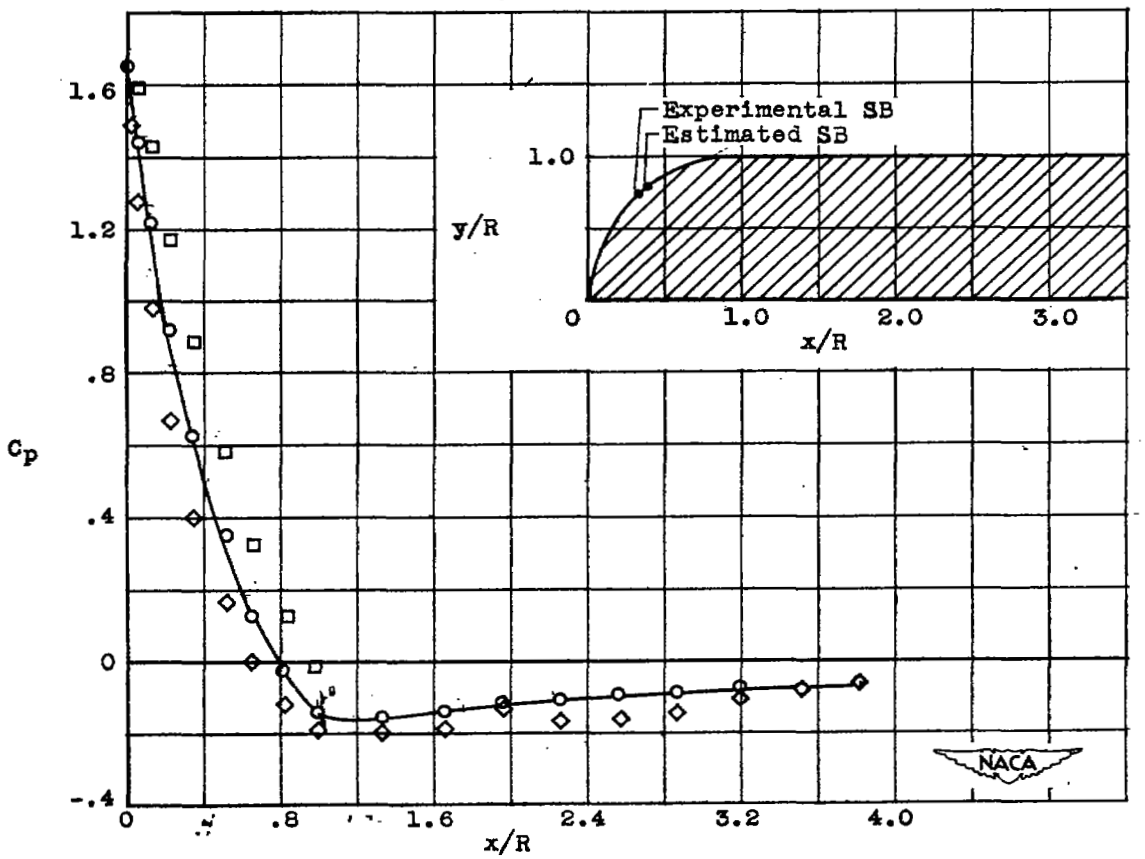


(b) Body B-2.

Figure 10. - Continued. Pressure distribution over axially symmetric bodies. Free-stream Mach number, 1.9.

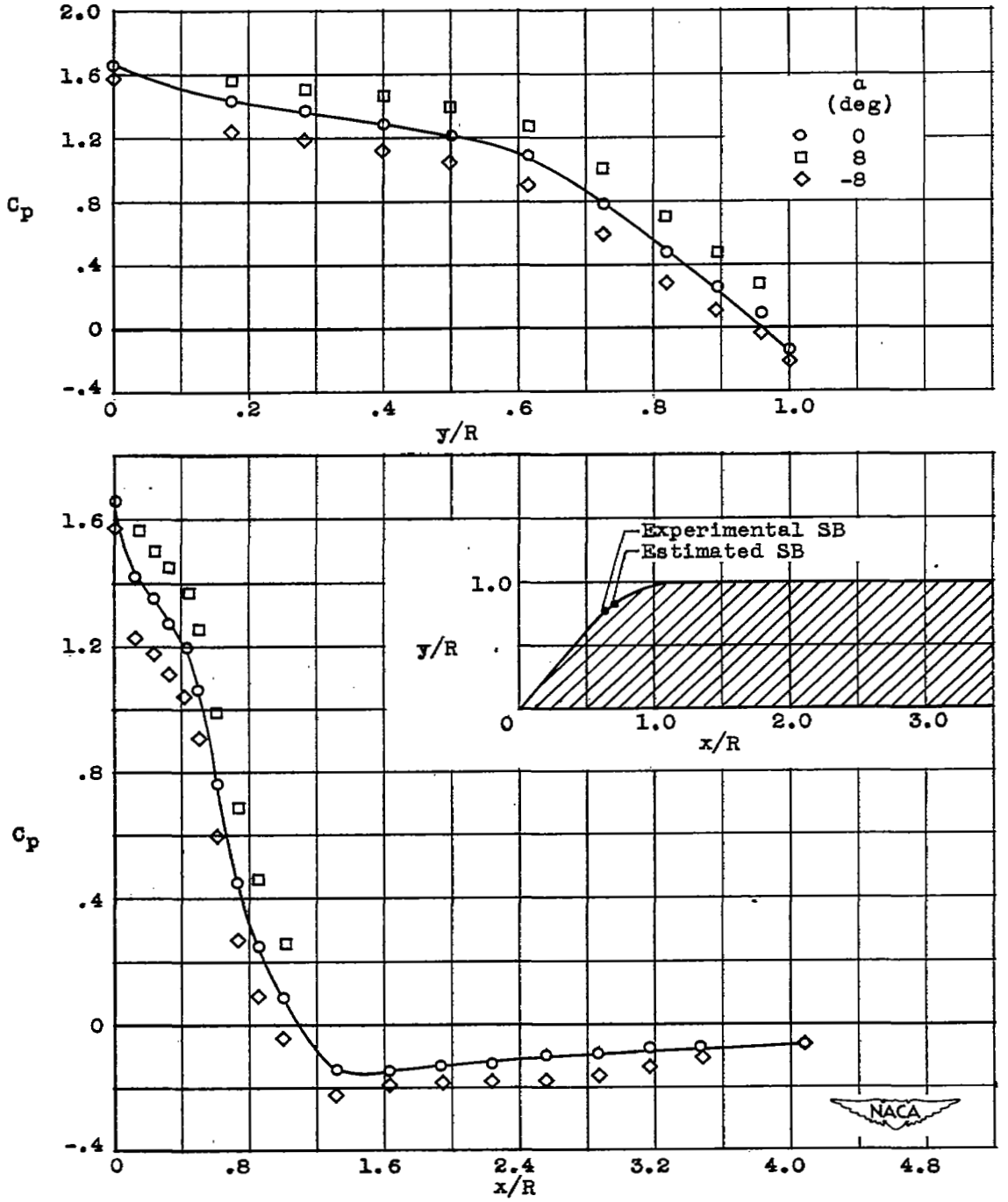


(c) Body B-3.

Figure 10. - Continued. Pressure distribution over axially symmetric bodies. Free-stream Mach number, 1.9.

[redacted]

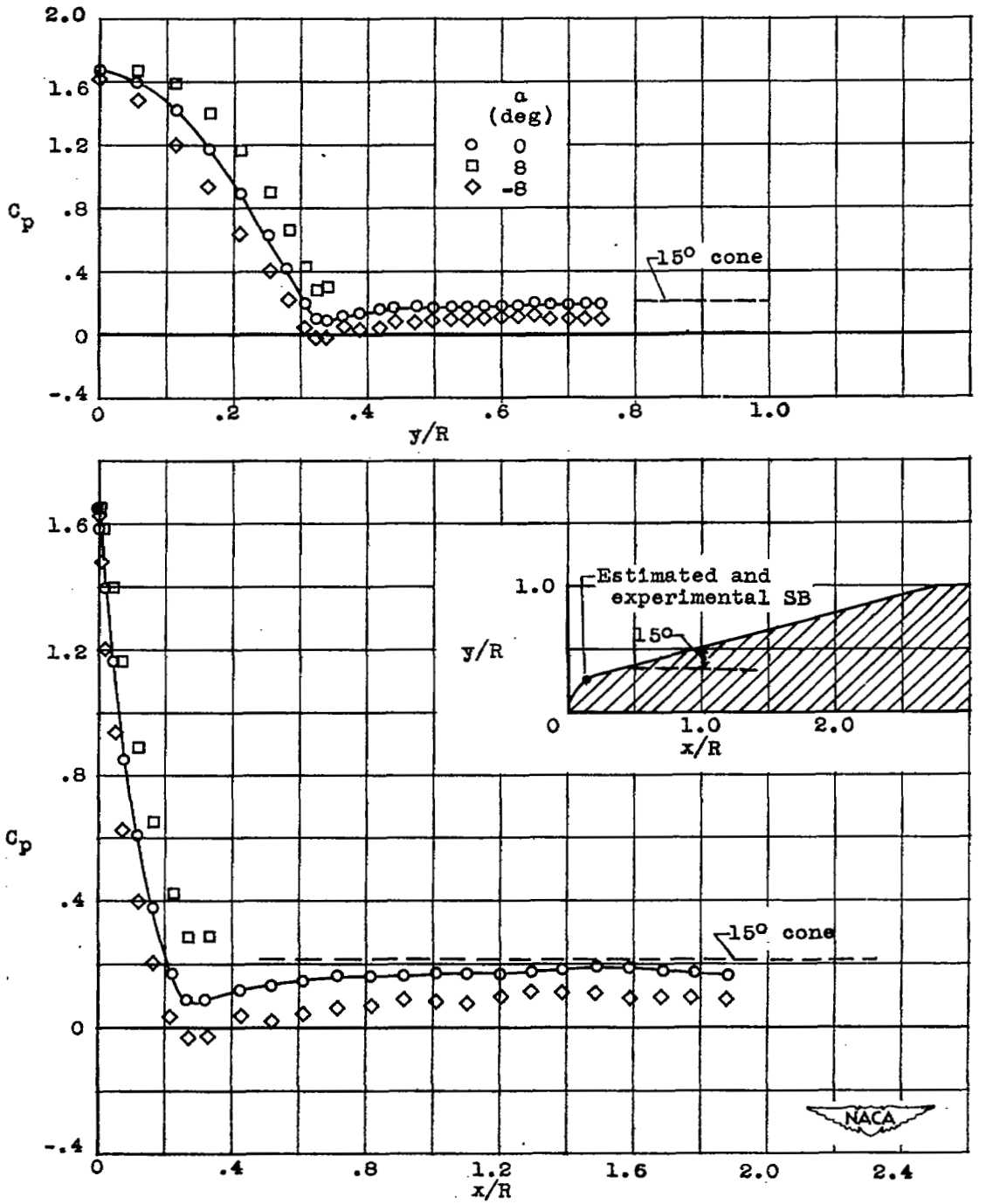


(d) Body B-4.

Figure 10. - Continued. Pressure distribution over axially symmetric bodies. Free-stream Mach number, 1.9.

1292

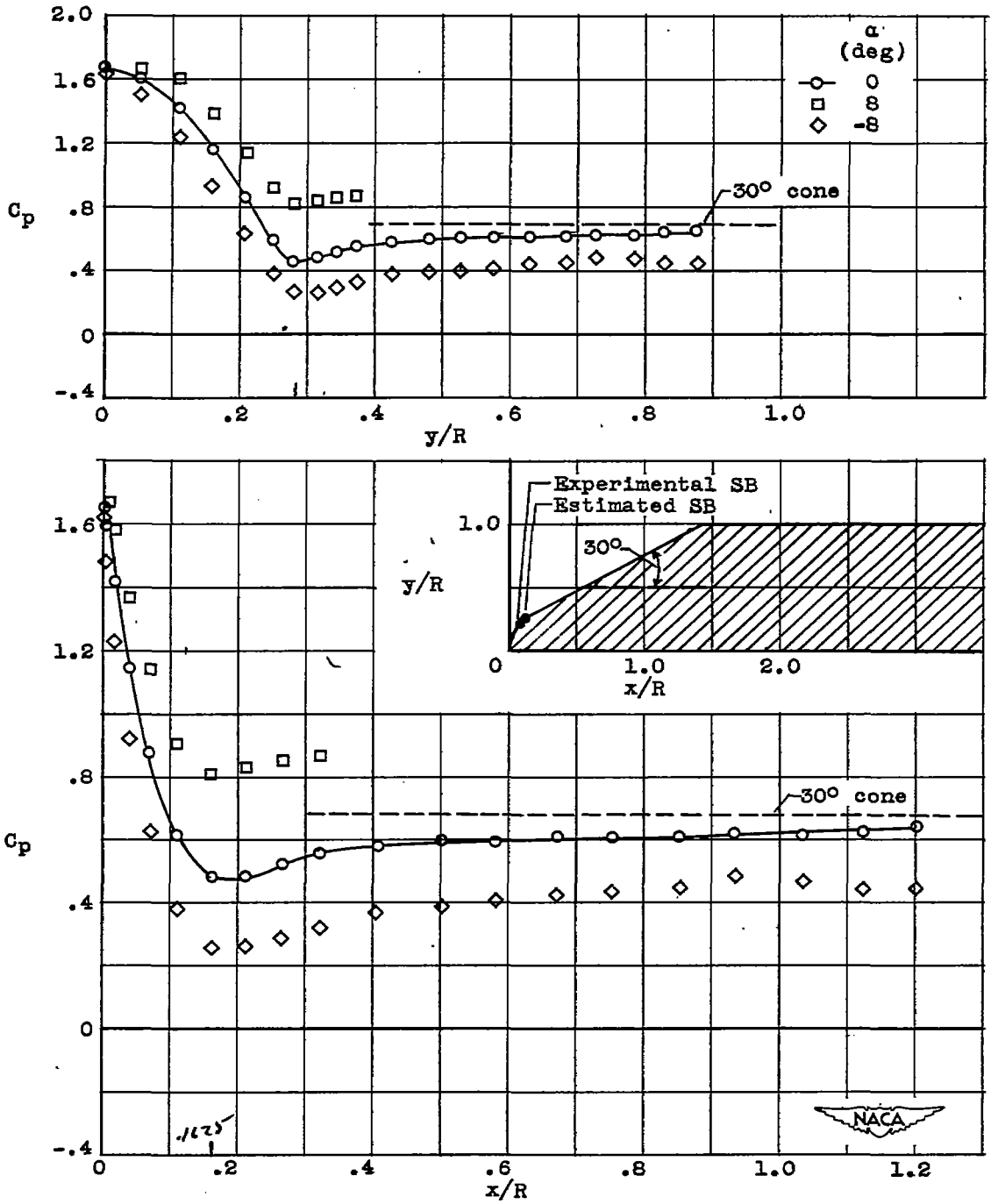


(e) Body B-5.

Figure 10. - Continued. Pressure distribution over axially symmetric bodies. Free-stream Mach number, 1.9.

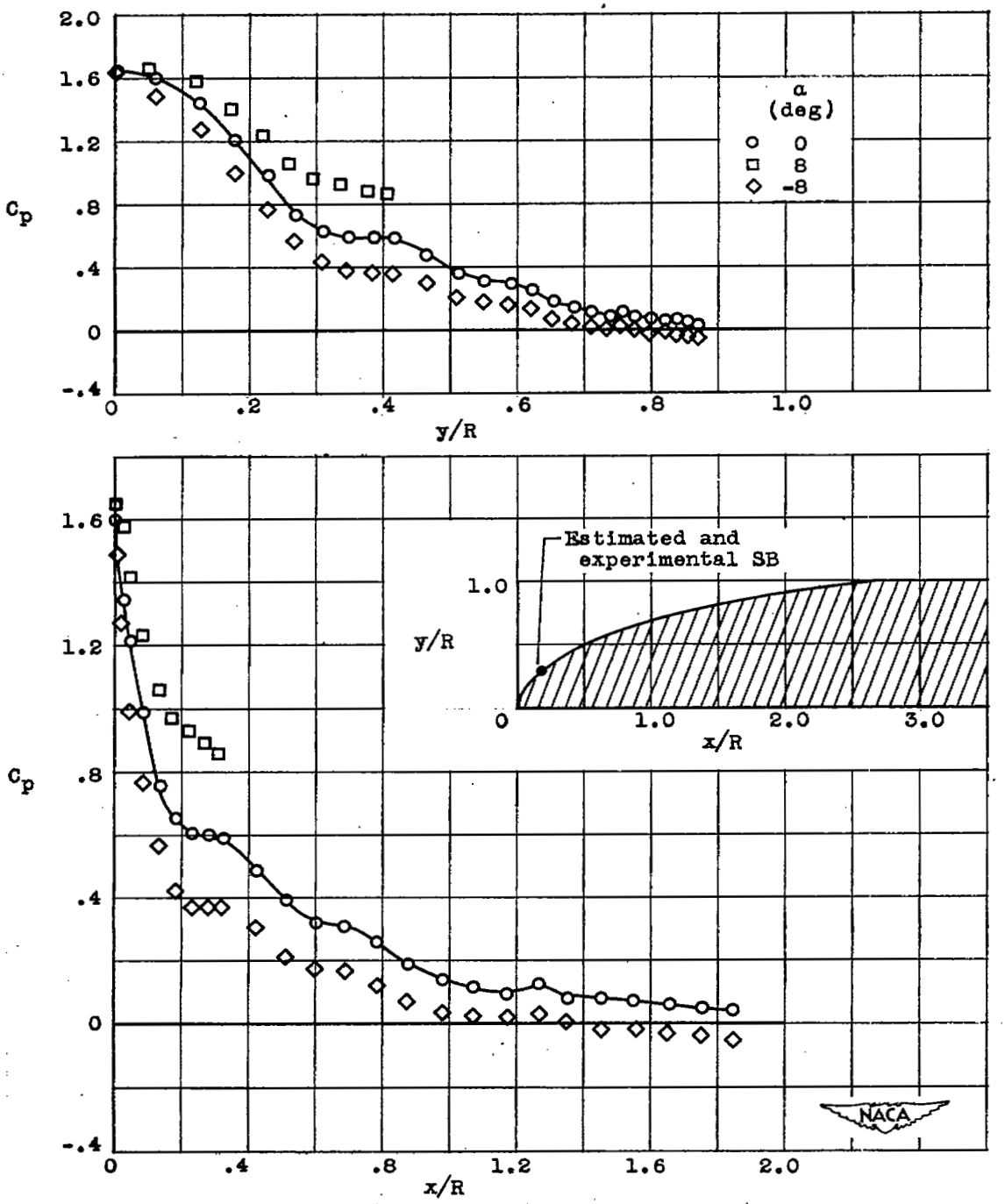


(f) Body B-6.

Figure 10. - Concluded. Pressure distribution over axially symmetric bodies. Free-stream Mach number, 1.9.

[redacted]

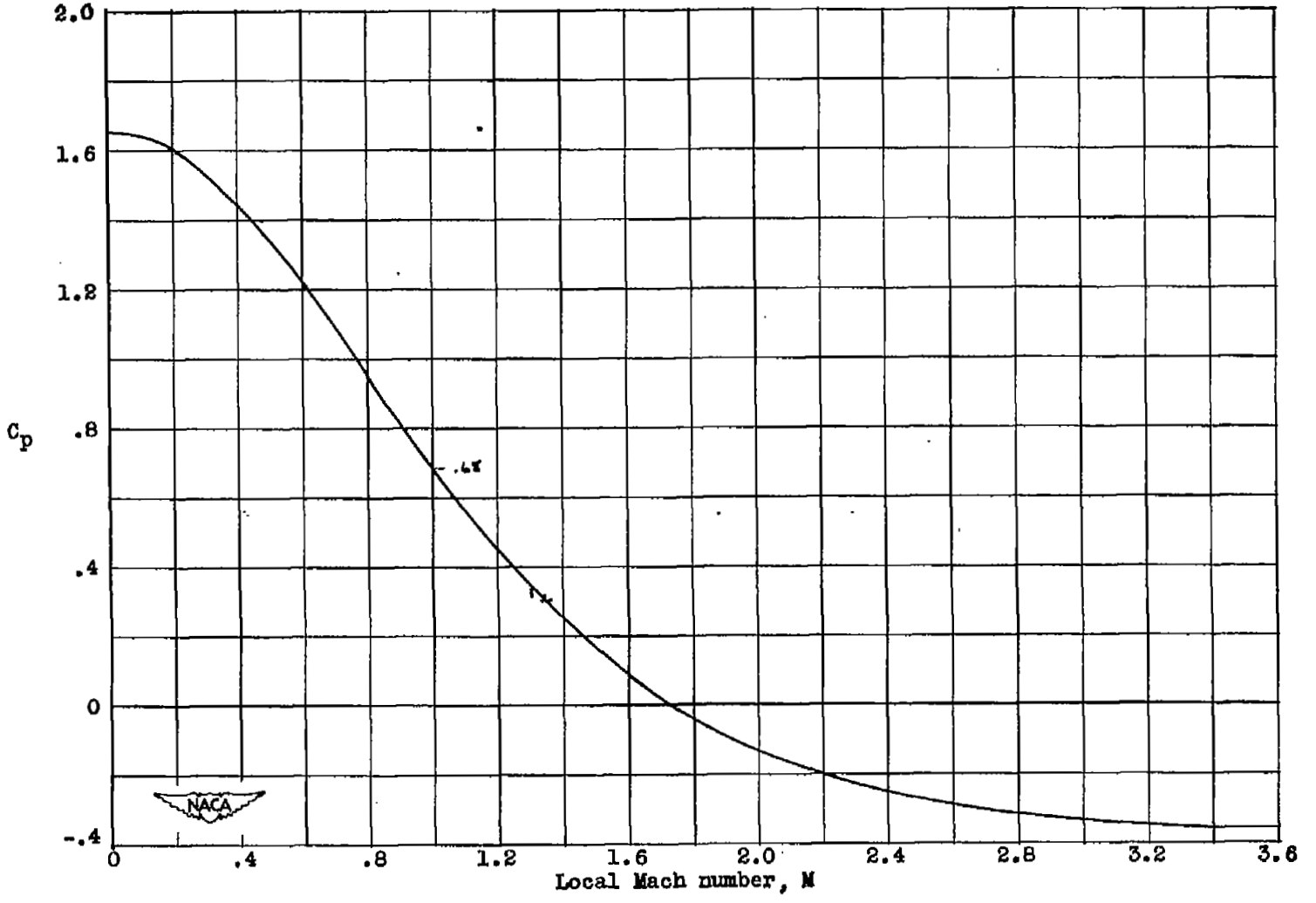


Figure 11. - Local pressure coefficient as function of local Mach number. Free-stream Mach number, 1.9.

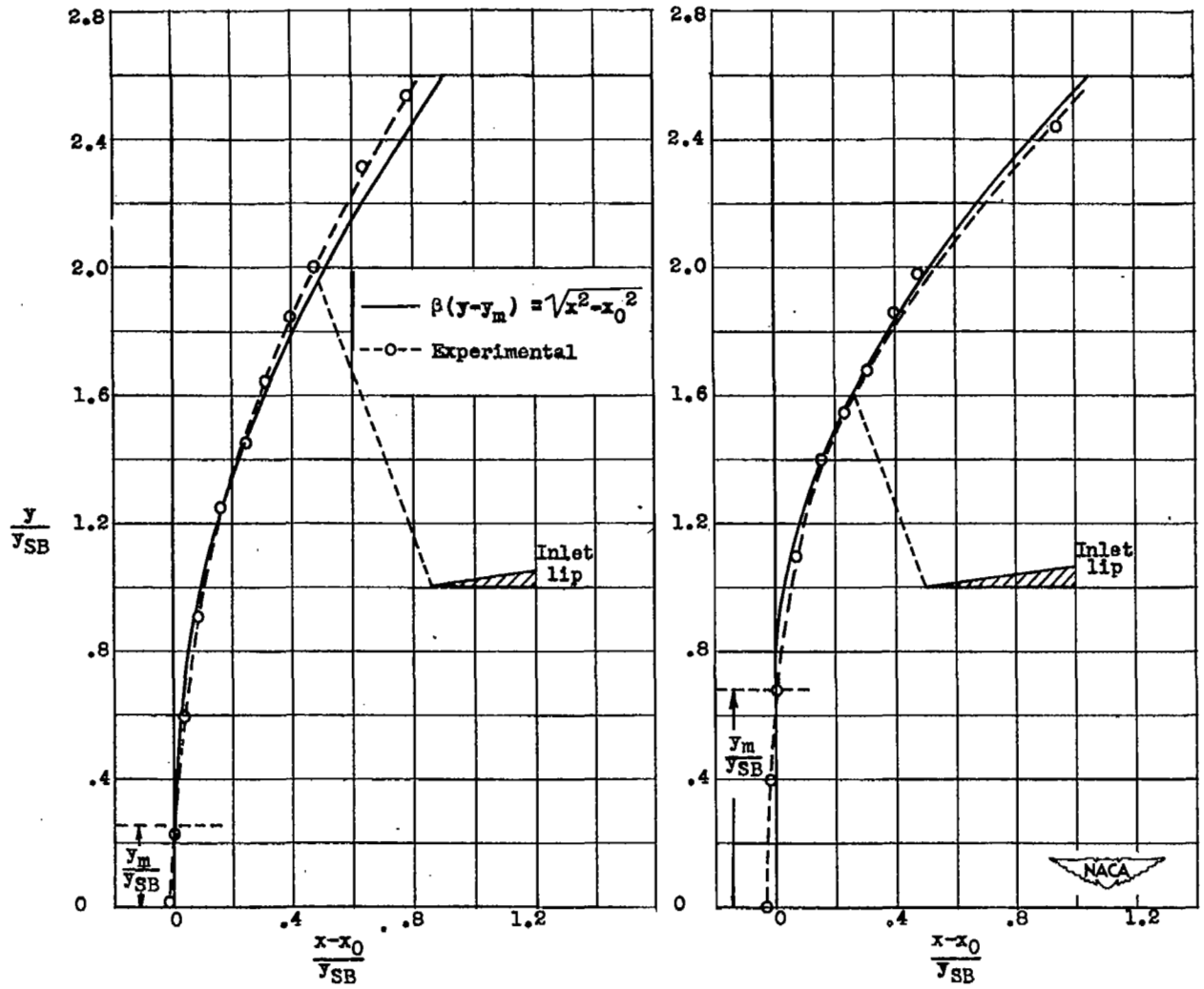


(a) Convergent inlet. (See fig. 3(m).)

(b) Convergent inlet. (See fig. 3(n).)

Figure 12. - Experimental and theoretical shock form upstream of several inlets. Free-stream Mach number, 1.9.

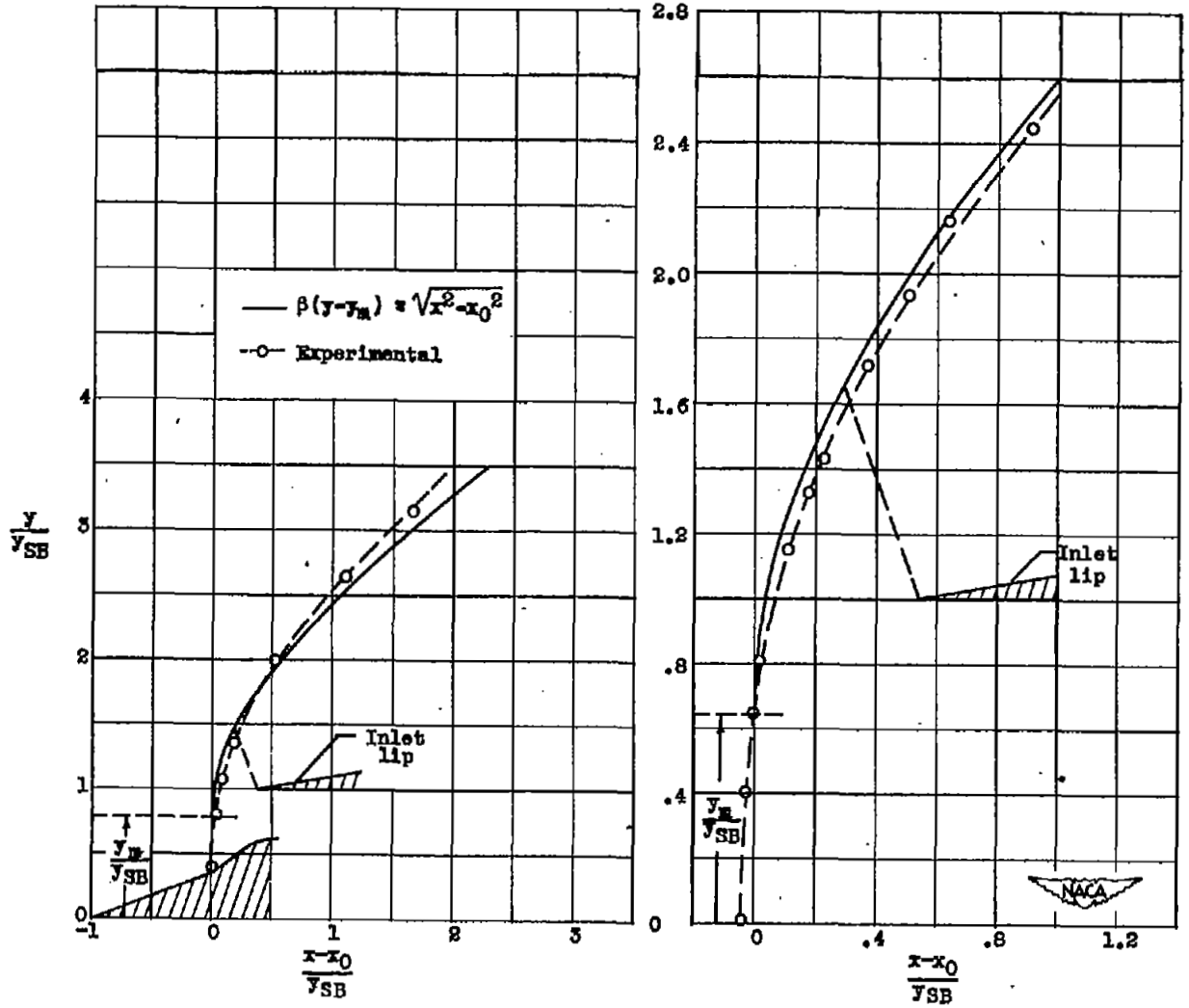


(c) Projecting island. (See fig. 3(o).)

(d) Perforated inlet. (See fig. 3(p).)

Figure 12. - Concluded. Experimental and theoretical shock form upstream of several inlets. Free-stream Mach number, 1.9.

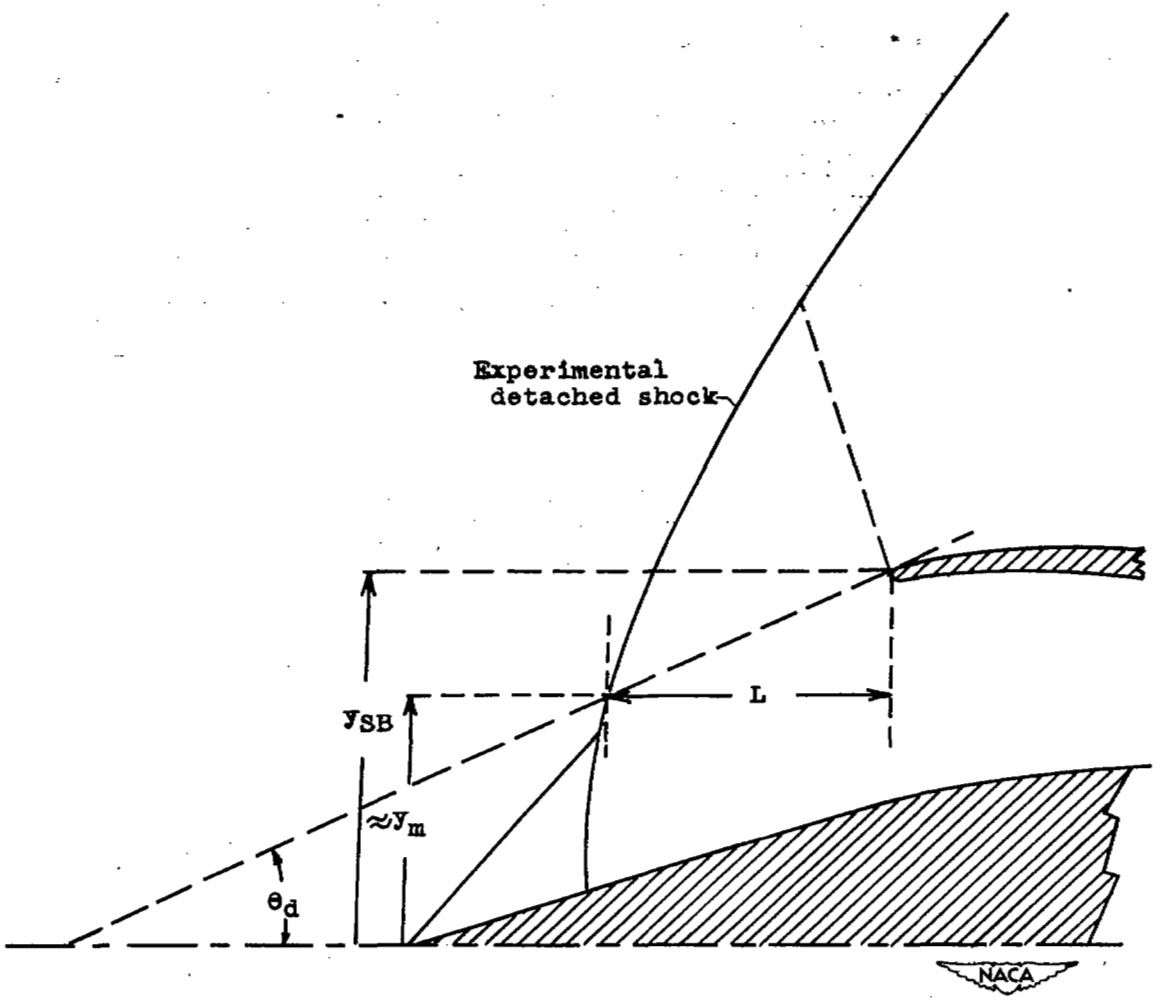


Figure 13. - Procedure for measuring relative shock location for computation of mass spillage and additive drag.

[redacted]

NACA-Langley - 7-5-50 - 400